BSPE98417-2183-1

Role of Polar Dust in Glacial-Integlacial changes using Paleoclimatic Ice-core Data

2012년 1월

한국해양연구원

제 출 문

한국해양연구원 원장 귀하

본 보고서를 “Role of Polar Dust in Glacial-Integlacial changes using Paleoclimatic Ice-core Data” 과제의 기획보고서로 제출합니다.

2012 년 1 월

과제책임자: 국종성
참여연구원: Fabrice Lambert
박종연

1. Research necessity

A. Scientific background

Mineral dust aerosols influence Earth's climate directly by scattering and absorbing incoming solar and outgoing longwave radiation. Indirectly they provide micronutrient-limited areas of the oceans with iron oxide and thus increase the amount of carbon that is absorbed into ocean waters. They also act as condensation nuclei for clouds and therefore influence the planetary albedo and the hydrological cycle. In turn, dust enthrallment and transport in the atmosphere is influenced by the climate. Ground vegetation, wind speed, and washout in the atmosphere limit the amount of dust that reaches the upper troposphere and is transported over long distances.

In the 2007 IPCC report, dust aerosols have been found to have a cooling global effect on Earth's climate. The error bars are very large though, and well-defined quantitative assessments of the effect of dust on radiative forcing are necessary to constrain it's uncertainty.

Dust flux from the atmosphere to the ground is measured in several climatic archives (i.e. terrestrial loess deposits, marine sediments, ice cores). In a bid to improve our knowledge of past climatic changes, the European Project for Ice Coring in Antarctica (EPICA) has yielded a wealth of information and data from the two ice cores drilled in opposite sites of the Antarctic ice cap. The dust records from the Dome C ice core offers the opportunity to investigate dust flux changes at an unprecedented resolution in the past 800,000 years.

B. Economic Impact

Improving our understanding of climatic processes is a key step in predicting climate change and thus prepare the economy for mitigation and modified environmental conditions.

C. Social Impact

Climate change mitigation should result in targeted measures that only the society at large can implement. An improved understanding of climatic

processes will help to foresee these measures enable the government to prepare the public for such changes.

Specifically, understanding how Earth's climate may react to a dustier environment is important to improve the climate models we use to predict future trends.

2. Current status of Domestic and International Researches

A. Domestic

Although there is a large climate-modeling community in the Republic of Korea (ROK), there is very little paleoclimatic research. This project will help opening new areas of research in the ROK and increase cooperation with foreign countries.

B. Foreign

Paleoclimatic research and especially ice-coring is a very advanced science in the European Union, the United States of America, Russia, and Japan, each of which have their own ice-coring teams and stations in the Arctic and/or Antarctic polar caps. Recently, China has also intensified it's effort in this area and is planning ice-coring projects.

EPICA is a joint project between the science agencies of 10 European nations (Belgium, Denmark, France, Germany, Italy, Netherlands, Norway, Sweden, Switzerland, UK) and the European Science Foundation. Two ice-cores were drilled at the opposite sides of the Antarctic polar cap: The first at Dome Concordia (Dome C) on the East Antarctic Plateau, and the second in Dronning Maud Land (DML) facing the South Atlantic Ocean. The ice core at Dome C yielded the oldest ice ever recovered (800'000 years), whereas the DML ice-core permits North-South Atlantic comparison with Greenland ice-cores.

A new project involving China, the EU, and the US is in preparation in the

vicinity of the Chinese Kunlun Station (Dome A) to drill and ice-core that will hopefully recover ice of over 1 Million years of age.

Continuous time series of dust flux are available from loess deposits, marine sediment cores, and glacier and polar ice cores. Among these, polar ice cores are prized because of their high temporal resolution and the reasonable length of the record (loess and marine sediment records go much further back in time). Several studies have been published on Greenland dust records from ice cores at GISP, GRIP, and NGRIP. In Antarctica, dust records from Vostok and Dome C have been published at low resolution, focusing on broad climatic relations.

Dust models are usually atmospheric aerosol models coupled to general circulation models. They provide snapshots of atmospheric dust concentrations under specific conditions. Most notably, they have been used to assess atmospheric dust concentrations not only under modern conditions, but also in glacial conditions or during predicted future climates with higher greenhouse gas concentrations. The estimation of present and past global dust concentrations has so far only been done with dust models.

3. Objectives

a) Main Objectives

This project has two main objectives. The first focuses on the interpretation of high-resolution dust data from the EPICA - Dome C ice core. Statistical analysis of soluble and insoluble dust proxy records will be performed. In addition, the behavior of dust during glacial-interglacial climatic transitions will be compared with the changes in temperature, greenhouse gases, and ocean sea-level back to 800,000 years BP.

The second objective is to produce an estimate of present and glacial atmospheric dust concentrations based on paleoclimatic data. The idea is to gather dust flux data from all paleoclimatic data sources where dust flux is available for both the Holocene and the Last Glacial Maximum periods. Using a kriging algorithm, these single points on the globe will be interpolated to a continuous grid. It will then be possible to combine the gridded data with results

from dust climate models, and to produce an alternative dataset of dust concentrations for both present and very dusty conditions. This dataset can then be compared with model results and will possibly point to areas where models may be improved. In addition, a focused analysis of dust impact on radiative forcing in polar areas, where dust models generally show performance problems, may help to understand polar phenomenons like the polar amplification.

The success of this project should result in one ore more publications in scientific journals.

b) Research content

A Continuous Flow Analysis system (CFA) was used to measure trace element and dust concentrations in the EPICA ice-cores. These measurements yielded data sets at 1 cm resolution, resulting at Dome C in sub-annual time resolution at the top of the ice-core to ~25 year resolution at the bottom. For the first time, sub-millennial variability can be investigated in the past glacial-interglacial cycles. Past manifestations of fast climatic variations like Dansgaard-Oeschger events and their corresponding Southern Hemisphere counterparts, the Antarctic Isotopic Maxima, may be recorded in the CFA data set. The unprecedented resolution of this dataset will hopefully allow to confirm if such events happened during all glacial periods or only the last. The identification of past warming events during past glacials may increase our knowledge about these phenomenons and allow improved models.

On a global average dust concentrations in the air are generally 3-4 times higher during glacial times than during interglacials due to enhanced aridity, reduced hydrological cycle, and increased wind speed. However, glacial aeolian dust depositions in the polar caps increase by an order of magnitude compared to interglacial levels. Aerosols have been shown to have a net negative impact (direct and indirect) on radiative forcing. Thus the very large increase in airborne dust particles in high latitudes should have helped to cool down the polar caps and was a force against warming changes. This cold positive reinforcement of dust in polar areas will be investigated using a combination of

ice core and dust model data in a one-dimensional rapid radiative transfer model. In addition, a global estimate of dust-induced radiative forcing will be produced using a global reconstruction of atmospheric dust concentrations.

c) Methodology and research strategy

Since all of the data have been already measured, this project does not require field work. Most of the published data from the Dome C ice core so far is at a 55 cm depth resolution, which corresponds to a time resolution of 10 years at the top, and ~1000 years at the bottom of the core. The 1 cm resolution CFA data is published down to 1960 m depth or 173'000 years age, the lower part being unpublished yet and will thus require approval by the University of Bern for use. Since I (Fabrice Lambert) was the one who measured and compiled these data, I do not expect any problems in cooperation with the University of Bern.

For the global reconstruction, the recently published DIRTMAP 3 dataset will mainly be used. New results of dust flux during the Holocene or the Last Glacial Maximum will be added as they are published.

3. Expected impact

A. Scientific impact

The publication of the high-resolution Dome C data will be welcomed by all the paleoclimate community. These data will improve our understanding of past climatic processes during glacial-interglacial transitions, as well as of the centennial and millennial variability in the Southern Hemisphere during the past 800,000 years.

The role of mineral dust in the climate is little understood. Climate models have consistently failed to reproduce glacial dust concentrations at high latitudes. In addition the radiative forcing effect of dust is burdened with a very large uncertainty. The successful completion of this project will improve the understanding of the impact that mineral dust has on climate, especially at high latitudes.

B. Economic and social impact

By improving our knowledge of climatic changes in the past, modeling of future climate will be more detailed, robust, and trustworthy. Society at large will profit from this knowledge by being better prepared for the challenges that future climate change holds.

4. Results

A. Centennial mineral dust variability in high-resolution ice core data from Dome C, Antarctica

1. Introduction

Atmospheric aerosol production, mobilization, long-range aeolian transport, and deposition respond to past climatic changes (Fischer et al., 2007a, 2007b; Legrand and Mayewski, 1997; Mahowald et al., 2006a; Wolff et al., 2006). Vice versa, dust and other aerosols affect radiative forcing, thus climate, through absorption and scattering of radiation (Mahowald et al., 2006b; Miller and Tegen, 1998; Tegen et al., 1996) and play a role as condensation nuclei (Sassen et al., 2003; Schwartz, 1996). The total atmospheric dust load, as well as physical (e.g. size, shape) and mineralogical characteristics are important factors for the radiative budget of the atmosphere (Tegen, 2003), and for the micronutrient supply to terrestrial and marine ecosystems (Martin et al., 1991). The hypothesis that a reduced supply of iron to the Southern Ocean could be responsible for a substantial part of the 80-100 ppmv CO_2 increase from the Last Glacial Maximum (LGM) to the Holocene has been discussed for some time (Martin et al., 1990; Watson et al., 2000). Estimates for the contribution of this iron fertilization to the total glacial/interglacial CO_2 difference range from <20% to <40% (Bopp, 2003; Ridgwell, 2003; Röthlisberger et al., 2004). It is commonly believed that a combination of iron fertilization, carbonate compensation feedback, and Southern Ocean ventilation changes together with

changes in ocean temperature drives the glacial-interglacial CO_2 changes (Fischer et al., 2010; Köhler and Fischer, 2006; Köhler et al., 2005; LeGrand and Alverson, 2001; Sigman et al., 2010; Watson and Naveira Garabato, 2006). Accordingly, documenting the centennial to millennial variability in dust input into the atmosphere and into the Southern Ocean is of great importance to constrain the impact of dust on the radiative budget and iron fertilization.

Insoluble mineral dust particles (dust) and soluble ionic aerosol constituents, such as calcium (Ca^{2+}) and sodium (Na^{+}), are transported through the atmosphere also to remote polar areas, like the central East Antarctic plateau (Fischer et al., 2007b; Wolff et al., 2006). Many of these aerosol species (such as mineral dust) are non-volatile and irreversibly deposited onto the ice sheets (Legrand and Mayewski, 1997). Thus, they are regularly measured in polar ice cores and allow for conclusions concerning climatic processes in the aerosol source region and during transport in the past.

In the case of mineral dust, long-term changes have been documented during the last 800,000 years in low-resolution dust records from the Dome C ice core, Antarctica (Lambert et al., 2008) showing extraordinarily high dust fluxes during glacial conditions. Strontium and neodymium isotopic analysis identified southern South America (>32°S) as the primary source for dust deposited onto the Antarctic ice sheet during recent climatic periods (Delmonte et al., 2004) with a strong relative contribution from possibly Australian sources during recent

interglacials (Delmonte et al., 2008; Revel-Rolland et al., 2006), and a possible additional source in the Puna-Altiplano in Argentina during glacials (Delmonte et al., 2010; Gaiero, 2007). The contribution of the exposed continental shelves during glacial times is unclear (Bigler et al., 2006; Maher et al., 2010), however, comparison of the temporal evolution in dust aerosol tracers and sea level during the last termination rules out that flooding of the previously exposed Argentinian continental shelf was the dominant factor for the dust changes during that time (Wolff et al., 2006).

Because calcium was more rapidly measurable at high resolution in polar ice cores than particulate dust, it has routinely been used uncorrected (Ca^{2+}) or corrected for its sea salt contribution ($nssCa^{2+}$) as a proxy for aerosol dust deposited in central Greenland (Fuhrer et al., 1999; Mayewski et al., 1994) or in central Antarctica (e.g. (Fischer et al., 2007a; Röthlisberger et al., 2002). Particulate insoluble dust volume has been measured by the Coulter Counter technique (e.g. (Delmonte et al., 2002)) at low resolution. Since 1999 laser-absorption was used for high resolution particulate dust measurements (Ruth et al., 2002), however, size calibration of the absorption measurements is still a matter of discussion.

In this study we present for the first time the complete datasets of Ca^{2+}, $nssCa^{2+}$, and insoluble dust records (based on laser absorption measurements) from the Dome C ice core at 1 cm resolution spanning the entire past 800,000 years,

obtained in the frame of the European Project for Ice Coring in Antarctica (EPICA). The calcium to particulate dust relationship is investigated during glacials and interglacials. Using Principal Component Analysis (PCA), we produced a common dust flux signal that exhibits joint features of all our three dust proxy records. These new dust flux data are used to analyse millennial variability in the past eight glacial periods. We also investigate the possible causes and effects of dust variations and stepwise dust changes during glacial terminations.

2. Methods

The EPICA Dome C (EDC) ice core was drilled in East Antarctica (75°06'S; 123°21'E) and covers the last 800,000 years (Jouzel et al., 2007). From a depth of 24.2 m down to 3200 m a Continuous Flow Analysis (CFA) system (Bigler et al., 2006, 2010; Kaufmann et al., 2008; Röthlisberger et al., 2000) was applied to measure, among others, insoluble dust particles and soluble Ca^{2+} and Na^{+}. The data gathered with this method have a nominal depth resolution of ~1 cm taking dispersion in the CFA system already into account, which corresponds to a formal sub-annual temporal resolution at the top and up to ~25 years at the bottom of the ice core. Practically, surface snow mixing and dispersion in the ice result in a lower effective temporal resolution.

2.1 Calcium and non-sea-salt Calcium

For the ionic constituents the detection limit was about 0.2 ng g^{-1} for Ca^{2+} and 3 ng g^{-1} for Na^{+} (Bigler et al., 2006). The mean error for both Ca^{2+} and Na^{+} is estimated to be lower than ±10% (Bigler et al., 2006; Röthlisberger et al., 2000).

In contrast to particulate dust, Ca^{2+} has, apart from terrestrial, also marine sources (Bigler et al., 2006; Legrand and Mayewski, 1997). Although the marine aerosol ratio of Ca^{2+} to Na^{+} is well known (Bowen, 1979), few studies have investigated the continental Ca^{2+} to Na^{+} ratio of terrestrial aerosols from specific regions (i.e. southern South America) (Bigler et al., 2006). However, these ratios are needed to calculate the exclusively terrestrial non-sea-salt calcium based on Ca^{2+} and Na^{+} measurements. The sea-salt (ss) and non-sea-salt (nss) contribution to Na^{+} and Ca^{2+} can be calculated using the system of linear equations

$$[ssNa^{+}]=(R_t*[Na^{+}]-[Ca^{2+}])*(R_t-R_m)^{-1}$$

and

$$[nssCa^{2+}]=R_t*([Ca^{2+}]-R_m*[Na^{+}])*(R_t-R_m)^{-1},$$

with R_t and R_m being the terrestrial and the marine Ca^{2+}/Na^{+} ratio, respectively (Bigler et al., 2006; Röthlisberger et al., 2002). Traditionally, the ratio R_m was assigned to the marine bulk sea water ratio of 0.038 and R_t to the average

crustal value of 1.78 (Bowen, 1979). However, other sources than sea spray, such as frost flowers, may have contributed significantly to the marine ion concentrations in central East Antarctica (Wolff et al., 2006). Based on these assumptions, an R_m value of 0.044 was proposed for Antarctic ice core data (Rankin et al., 2000). A study by Bigler et al. (2006) that estimated these ratios empirically using high-resolution CFA data from Dome C found R_m = 0.043 ± 9% and R_t = 1.06 ± 8% for the East Antarctic plateau. The lower R_t value compared to Bowen (1979) most likely reflects the local crustal composition in southern South America. We used the marine and terrestrial Ca^{2+}/Na^{+} ratios from (Bigler et al., 2006) in this study. Note that the difference in these parameters only marginally affects the calculation of nssCa^{2}+ in contrast to sea salt Na^{+}, which is not discussed here. Calcium and sodium data below the detection limit were discarded. Values below 0.1 ng/g (including all negative values) in the nssCa^{2+} record were also discarded to avoid artefacts produced by exceptionally high sodium concentrations, as the ratios R_t and R_m are in principle only valid on average, and might not apply to single data points. Assuming an error of 10% for Ca^{2+}, Na^{+}, R_m, and R_t, the uncertainty of the nssCa^{2+} record amounts to ~0.2 ng/g (30%) during interglacials and ~5.4 ng/g (10%) during glacial maxima.

An additional analytical concern may be the amount of Ca^{2+} being leached from particulate dust after the ice sample has been melted. This amount may be dependent on the acidity of the sample. Anomalously high Ca^{2+}/dust ratios were found coinciding with volcanic eruptions (Ruth et al., 2002) in Greenland ice

samples with very high Ca^{2+} concentrations. However, these occurrences are very localized and rare, and do not influence the long-term signal. In addition, the very good correspondence of Ca^{2+} concentrations measured by CFA and traditional ion chromatography (IC) (Ruth et al., 2008) excludes that a systematic offset is introduced during the CFA measurements. In case of IC measurements, the melted sample gets in contact with the acidic IC eluent, which would lead to a higher solution of Ca^{2+} from particulate dust if this were to be an important effect. Only for very low Ca^{2+} concentrations does the IC data divert to somewhat higher concentrations. However, this is due to the higher analytical blank of the discrete IC analysis. Accordingly, the CFA measurements can be regarded as reliable data of Ca^{2+} concentrations in ice core melt water. Note, that this does not exclude a potential temporal variation in Ca^{2+} leaching of dust aerosol during atmospheric transport.

2.2 Insoluble dust

Insoluble dust concentration and size distribution below 769.5 m (from 44 to 800 kyr BP) were measured by laser-absorption particle sensors and counters (Abakus from Klotz, Germany) (Ruth et al., 2003), in the following denoted as Bern dust data. The particle size detection limit of these laser particle devices (LPD) is approximately 1 μm of equivalent spherical particle diameter. The upper measuring limit was set to 17.2 μm. Within this size range the LPD counts the number of particle in 32 different size channels. The sum of all channels is then converted into an analogue voltage signal. In the Bern dust data this

voltage signal was converted to number of particles per millilitre as described in (Bigler, 2004). The first 769.5 m were measured with a custom-made LPD from the University of Copenhagen featuring 4 channels only, and are referred to in the following as CPH dust data.

In principle, the particle size channels can be calibrated with spherical latex particles. In practice, however, this calibration proved insufficient, as mineral dust particles come in all shapes. Therefore, only the total dust particle number was used in this work and an empirical calibration to dust mass fluxes was performed (see below) using low resolution Coulter Counter data (Lambert et al., 2008). Note that this calibration does not allow for a quantitative interpretation of dust size changes derived with the LPD. The error of the LPD dust particle number data is estimated at <10% (Ruth et al., 2002).

The lowest part of the ice core (below 3000 m) had many cracks and breaks bearing the risk of contamination with drill fluid, whereas the rest of the core up to the end of the brittle zone (at ~950 m) was essentially break free. Contamination with drill fluid compromises both LPD and CC measurements. They caused either saturation of the LPD signal or were clearly recognizable based on unreasonably large size distribution data. In addition, the stratigraphy of the ice below 3190 m was disturbed and the climatic relevance of data collected in that part is strongly questioned (Jouzel et al., 2007). Therefore, only the data down to 3190 m depth are considered in this study.

2.3 Principal Component Analysis

The Ca^{2+}, $nssCa^{2+}$, Bern, and CPH dust particle number data are presented in Figure 1. The light grey curve shows the 1 cm high-resolution data, the superimposed black curve shows discrete 55 cm median values. Note that the Bern and CPH particulate dust data have separate y-axes. All three species are considered a proxy for atmospheric mineral dust concentrations, each with its own advantages and limits. Calcium has a low uncertainty, but is "contaminated" with $ssCa^{2+}$ during interglacials. The correction to $nssCa^{2+}$ removes the sea-salt part at the cost of a lower accuracy due to the choice of R_t and R_m and a larger scatter at low concentrations. LPD particle number data have a low uncertainty for most of the record, but are not easily calibrated to mass concentration units. Principal Component Analysis (PCA) (e.g. (Abdi and Williams, 2010)) provides the means to extract the common climatic signal from all of these datasets. The low accumulation rate at Dome C and the log-normal distribution of dust proxy data make the logarithmic values of fluxes most representative for changes in atmospheric dust aerosol changes (Fischer et al., 2007b). Therefore, all datasets were multiplied with the accumulation rate and logarithmized prior to the PCA. Note that the accumulation rate is only available at 55 cm resolution (Jouzel et al., 2007) and that values in between were linearly interpolated.

In a first step, the CPH and Bern dust data had to be fused to one dataset. The CPH and Bern devices had different sensitivity which resulted in different

variability in the two data sections. To homogenize the two datasets, both were separated in a high-frequency and a low-frequency part by subtracting a smoothed curve (we used a 1 kyr running mean with $\cos^2$ shaped weights) from the logarithmized flux data. The two parts of the CPH data were then standardized (i.e. centred and divided by the standard deviation) using their respective mean and standard deviation, and de-standardized using the mean and standard deviation from the respective part of the logarithmized Bern data in the section 120-165 kyr BP. This time section was chosen because it is similar to the CPH data section in length and also encompasses both glacial and interglacial values. The resulting high and low frequency datasets were then added together and appended prior to the Bern data. We justify this procedure with the fact that both Ca^{2+} and $nssCa^{2+}$ show similar means and standard deviations (within 20%) in high and low frequency bands in these two data sections. Nevertheless, one should keep this feature in mind when analysing variability in the youngest part of the PCA-derived data.

The first principal component (PC1) explains over 92% of the variance in the records, and we interpret it as the climatic signal common to all three species. The rest of the variance stems from measurement uncertainty, sea-salt influence, and noise. Gaps in the Ca^{2+}, $nssCa^{2+}$, and LPD datasets were linearly interpolated prior to performing the PCA. The linear interpolation is a good approximation of the average value, thus the level of the PC1 data is not particularly affected. However, if there is a gap in one or two of the original

records, the variance in PC1 will be decreased in that section (Fig. 3b). One has therefore to be careful when using the PC1 data to study dust flux variability in sections that feature large gaps in any of the original records. We reintroduced gaps in the PC1 data where all three original datasets have no data.

2.4 Calibration

To calibrate the PC1 data to dust mass flux units we used a two-sided regression analysis between PC1 and the logarithmized dust flux data from Coulter Counter measurements. CC measurements were performed on discrete 7 cm long samples at least every 6 m, but mostly every 55 cm over the whole EDC ice core. CC data and method are described in detail in (Delmonte et al., 2002). The fit of the PC1 to the CC data was performed with averaged PC1 data of all 7 cm sections where CC measurements were available.

To estimate the error in the two-sided regression we used a Monte Carlo approach, where we created 1000 ensembles of data points which scatter around the regression line with a distribution defined by the residuals of the original data points with the regression line. Note that the thus derived errors in the regression parameters reflect only the uncertainty in the regression itself due to the scatter of the entire dataset but not the measurement error in each individual data point. This led to a Monte Carlo regression between logarithmic CC fluxes and PC1 according to

$\log_{10}$CC= (0.4925±0.0124) * PC1 + (0.1069±0.0065) with r^2 = 0.83, n=1028

This translates to a relative calibration error of <10% for the dust flux values in the measured range between 0.1 and 50 mg m^{-2} yr^{-1}.

Note that with this calibration we avoided the issue of size calibration of the laser dust sensor. On the other hand, we cannot interpret differences in the evolution of soluble and particulate dust fluxes any more using our PC1 derived dust flux data. We therefore calibrated the CPH and Bern LPD data also individually in a similar fashion with the CC concentrations (in ng g^{-1}) in order to compare particulate dust concentrations to calcium concentrations. The regression between logarithmic CC concentration and logarithmic Bern LPD data was calculated to

$\log_{10}$(CC mass*)* = (0.9084±0.0309) * $\log_{10}$(Bern LPD data) – (1.3276±0.1076) with r^2 = 0.85, n=519

whereas the regression between the logarithmic CC concentration and logarithmic CPH LPD data was

$\log_{10}$(CC mass*)* = (1.633±0.089) * $\log_{10}$(CPH LPD data) + (3.136±0.128) with r^2 = 0.80, n=273

This translates to a calibration error in the range of 30-40% and 40-50% for the

entire range of dust concentrations (approximately 3-1500 ng g^{-1}) for the Bern and CPH dust data, respectively.

3. Results and discussion

3.1 Long-term trends in the insoluble dust to calcium ratio

Calcium and insoluble dust both follow the major climatic cycles with higher concentrations during cold times. Figure 1 shows the EDC particulate dust, Ca^{2+}, and $nssCa^{2+}$ concentrations, both at 1 cm and 55 cm resolution on a depth scale. We record typical interglacial concentration values of 1-2 ng g^{-1} for Ca^{2+}, 0.5-1 ng g^{-1} for $nssCa^{2+}$, and 200 Particles ml^{-1} for insoluble dust. During glacial maxima, average insoluble dust particle number concentrations increase by over two orders of magnitude, while Ca^{2+} and $nssCa^{2+}$ average mass concentrations increase by a factor of about 30 and 60, respectively. The particulate dust flux changes by a factor of 25-30.

The different rates of glacial/interglacial decrease in soluble and insoluble particulate dust tracers indicates already a significant difference in the glacial and interglacial dust composition. The EDC Ca^{2+} to insoluble dust mass ratio fluctuates between about 0.04 and 0.2 (Fig. 2). The $nssCa^{2+}$ to insoluble dust mass ratio ranges between about 0.03 and 0.2, although the fluctuations are generally smaller than those in the Ca^{2+}/dust ratio. Low and high ratios are generally related to glacial maxima and interglacials, respectively. The lower LGM values may be due to different mineral compositions of dust transported to

the southern polar region during cold times. The higher interglacial values could be related to an additional dust input from Australian or even local Antarctic sources during warm times that becomes insignificant relative to the total dust deposition during glacial times. Interestingly, a clear change in dust composition has also been derived from He isotope measurements on mineral dust aerosol from the EPICA Dronning Maud Land ice core between the last glacial and the Holocene (Winckler and Fischer, 2006).

Alternatively, glacial Antarctic dust may have been subjected to a greater amount of Ca^{2+} leaching due to a change in weathering conditions on the way from its source, or affected by changing ice alkalinity (Ruth et al., 2002). The size of dust particles is unlikely to have played a role, as it stays fairly constant over the record, with glacial-interglacial changes of only 5% (Delmonte et al., 2004; Lambert et al., 2008). The fact that both Ca^{2+} to insoluble dust and $nssCa^{2+}$ to insoluble dust ratios show similar variability patterns, suggests that varying amounts of sea-salt calcium were not responsible for these changes.

It is interesting to note, that the calcium to insoluble dust ratio changes its pattern before 700,000 years BP. Taken at face value, these changes in the bottom part of the core point to a change in the crustal composition of dust transported to Antarctica during the climatic reorganization that happened at the Mid-Pleistocene Revolution. Note, however, that in this depth interval, single dust particles were agglomerated, possibly due to ice recrystallization and shear

deformation processes (Lambert et al., 2008). This could potentially affect the leaching of Ca^{2+} from these aggregates. Grain size data shows a trend towards larger ice crystals with increasing depth and may be influenced by dust content (EPICA comm. members, 2004). However, the low resolution of the physical properties data at this depth prevents a conclusive link between dust particle aggregates and ice crystal size.

3.2 High resolution dust flux changes

In Figure 3a we show the calibrated PC1 dust flux dataset. It is shown in black with the Coulter Counter dust flux data (Lambert et al., 2008) overlain in red. As the common signal found in the high-resolution particulate dust, Ca^{2+}, and $nssCa^{2+}$ data, PC1 can be interpreted as the best representation of high-resolution atmospheric mineral dust variability. Being empirically calibrated against dust mass fluxes from CC measurements, the amplitude of the changes reflects that of insoluble particulate dust fluxes. The dataset ranges from 400 to 801,000 years BP and is at 1 cm resolution. This corresponds to a formal three months resolution at the top to ~25 years at the bottom of the core. Average dust flux values vary between 0.2 - 0.6 mg m^{-2} yr^{-1} and 10 - 30 mg m^{-2} yr^{-1} during interglacials and glacials, respectively.

3.2.1 Antarctic warming events

Antarctic warming events like the ones reported in stable water isotope as intermittent Antarctic Isotope Maxima (AIM) during the last glacial period

(Blunier and Brook, 2001; EPICA comm. members, 2006) are periods of accumulating heat in the Southern Atlantic Ocean, most likely related to a weakening of the Atlantic Meridional Overturning Circulation (AMOC) during stadial conditions in the North Atlantic, and a rapid restart of the AMOC at the onset of Dansgaard-Oeschger (DO) events (Stocker and Johnsen, 2003). A recent study suggested that during the last glacial period, every DO event had a corresponding AIM (EPICA comm. members, 2006). Similar features have also been recorded in previous glacial periods, suggesting that millennial scale variability was a persistent feature during glacial periods (Jouzel et al., 2007; Loulergue et al., 2008; Martrat et al., 2007).

Antarctic dust flux and temperature variations are very well correlated during glacial times (Lambert et al., 2008). This tight link between dust and climate allows us to use our dust flux record as a first order indicator of high latitude millennial climate variability. In Figure 4 we present a 25-year average of the dust flux during glacial periods in black, underlain with the EDC temperature in grey. During the past 60 kyr Antarctic warming events have been identified using the EDC isotopic record (EPICA comm. members, 2006). Note that the lower resolution of the EDC δD data, as well as the smoothing of the isotope record by diffusion in the ice, limits the recognition of warming events in the deeper core. Our high-resolution dust mass flux record is not subject to these limitations. Even before 740 kyr BP, where aggregation of dust particles in the ice occurs, we see no major effect of this process on the dust mass flux

reconstruction. A comparison of the EDC δD data with our dust flux record during the last glacial period shows that all the AIMs can also be seen in the dust record. Using our dust flux data, we have identified the potential Antarctic warming events during every glacial period back to Marine Isotopic Stage (MIS) 18 and named them according to the MIS they occur in. The identification was performed by subtracting a 3 kyr running median from a 1 kyr running mean with $\cos^2$-shaped weights using logarithmic dust flux values that were centred and inverted. All positive sections in the difference record that were longer than 700 years and had an area > 1.5 were defined as warming events. The four parameters of the detection algorithm (length of the window and percentile value of the running percentile (we also tried other values than the median), length and area of the section in the difference record) were calibrated on the last glacial period so as to detect all and only the AIMs.

The detection method appears to produce very good results. All major and almost all minor events in the dust are detected. There are two possible exception at 261 and 366 kyr BP where potential events were missed by the algorithm. There are also some events (6.2, 6.12, 12.3, 16.4, 18.1) that appear dubious to the eye and may be false positives. We have compared our warming events with the predicted occurrence of DO events based on EDC isotopic data (Barker et al., 2011). The predicted DO events have been marked with a triangle in Figure 4. Back to 310 kyr BP the predicted DO events coincide very well with the imprint of Antarctic warming events in the dust data. However,

before 340 kyr BP the time resolution of the isotope data drops quickly to more than 300 years per 55 cm, and some smaller potential events are only found in our data. On the other hand, (Barker et al., 2011) classified some of the larger signals as two separate events, whereas they appear as single occurrences in our dust data.

In summary, millennial variability in the Southern Hemisphere was a persistent feature during all glacial periods in the past 800 kyr. The centennial to millennial climate variability in the Southern Ocean region prior to 340 kyr BP was somewhat higher than derived by (Barker et al., 2011), and more DO events are likely to have taken place at that time in the North Atlantic region. The rate of occurrence of Antarctic warming events is fairly constant around 2-3 events per 10 kyr. We confirm prior findings of a tendency towards maximal variability during intermediate climatic states and low variability during climatic extremes (Wolff et al., 2009). However, small events did happen regularly also during glacial maxima just prior of each termination, which suggests that the bipolar sea-saw was not completely inactive during those times.

3.2.2 Transitions

The unprecedented resolution of our dataset allows for a precise analysis of the timing of dust changes and leads and lags with other parameters during climate transitions. Figure 5 highlights the behaviour of mineral dust during the last nine glacial terminations. Dust flux is shown in brown at a 25 year resolution during

all transitions, with the 1 cm data in grey in the background. We compare it to the EDC isotope temperature record in black (Jouzel et al., 2007), the EDC and Vostok CO_2 stack in red (Lüthi et al., 2008), and global sea-level data in blue (Bintanja et al., 2005). Note that these datasets are not available in comparable resolution and that the sea level data are given on their individual age scale, compromising the identification of leads and lags between sea level and the ice core records.

Against common practice, dust has been plotted on a linear scale to emphasize at which point in time the flux had dropped to levels close to the interglacial minima, where subsequent changes should not have significantly affected iron fertilization to the Southern Ocean. This time value has been marked with a dashed vertical line. Although the precise moment when dust reaches interglacial levels can be argued about, it is clear that in all glacial terminations this moment was reached in dust flux well before temperature and CO_2 reached interglacial levels. The dust lead on temperature and CO_2 is surprisingly consistent around 4 kyr and much larger than the uncertainty in the gas age-ice age difference. It is also easy to see that although CO_2 and dust flux usually start changing at approximately the same time, CO_2 levels continue rising steadily long after dust has reached interglacial values. In addition, during every termination, CO_2 levels were still rather low by the time the dust-born iron supply to the Southern Ocean had been reduced to interglacial levels. This shows that the continuing increase in CO_2 after the dust drop cannot be related

to a reduction in iron fertilization. Termination I and V show the largest CO_2 concentration rise of ~30 ppmv at the time dust reaches interglacial levels, which corresponds to about 40% of the total change. Other terminations show much smaller CO_2 increases concurrent with the dust decrease. We can therefore confirm the conclusion of previous studies that found it unlikely that iron fertilization of the Southern Ocean played the most dominant role in CO_2 concentration changes during the last termination (Bopp, 2003; Ridgwell, 2003; Röthlisberger et al., 2004), and extend it to glacial terminations in general. It is more probable that the oceanic iron cycle saturates at some point and that other processes or nutrients limit further planktonic growth above a certain iron concentration (Fischer et al., 2010; Martínez-Garcia et al., 2011; Parekh et al., 2008).

A special feature of the dust flux is that in most cases it did not gradually change from glacial to interglacial levels as temperature and CO_2 did. During most terminations the dust flux data show one or more sudden very fast drops that happen within a few centuries (indicated by vertical arrows in Figure 5). These sudden jumps occur during all transitions, although they are not as pronounced during terminations I and V when the dust flux falls more gradually towards interglacial levels. Clearly, the amplitude of these jumps is not as marked when using logarithmic dust flux data (as justified by the approximately log-normal distribution of dust fluxes for constant climate conditions), but the jumps are still prominent with respect to the rapidity of the step-like changes.

Looking at the sea-level data we can see no distinct level that would consistently correspond to the fast drops in dust flux. It is therefore not clear that these dust jumps are the consequence of the Argentinian shelf being submerged, and dust sources on the shelf being suppressed. This is in agreement with isotopic findings that locate the main source of glacial dust on modern Patagonian and Argentinian mainland (Delmonte et al., 2010). Note, however, that the benthic $\delta^{18}O$ based sea-level reconstruction (Bintanja et al., 2005) and the Dome C ice core data are given on their individual age scales making an unambiguous quantification of the phase relationship highly uncertain, especially in the older terminations.

Another more likely reason for the fast decline of dust flux during glacial terminations is a sudden change in atmospheric circulation and the hydrological cycle over the dust source regions. Increased moisture in previously arid regions may have allowed vegetation to grow quickly, which would have significantly hindered the dust mobilization into the atmosphere. In addition, an enhanced hydrological cycle would have reduced the life time of airborne dust particles during transport by increasing washout, thus reducing the amount of dust exported to far away regions (Lambert et al., 2008).

One possible reason for such a sudden change in the hydrological cycle of southern South America could be a latitudinal shift or change in extension of the westerly wind belt connected to the deep pressure trough and the region of

intense cyclonic activity in the Southern Ocean. Dust mobilization in southern South America today is mainly occurring during summer, when precipitation is low and individual high wind events can pick up dust aerosol. High wind speeds are connected to cyclones passing the Drake passage and thus episodic in character (Lässig et al., 1999). Further to the north, zonal wind conditions crossing the Andes lead to Föhn conditions (Zonda wind) lee-sides of the mountains (Lässig et al., 1999), connected to high wind speed and potentially dust uptake. It has been suggested that the position of the Westerlies over South America varies according to sea surface temperature (Lamy et al., 2010). During cold conditions, the region of high westerly wind may expand northward (as is the case for recent winter conditions), making cyclonic influence in southern South America less episodic and zonal winds more steady. In addition, the dryer conditions during glacial times connected to a constant replenishment of fluvial dust source by enhanced glacial outwash, lead to a combination of high dust supply and strong wind uptake at that time. As temperature rises, the wind belt contracts, while the wind intensity in the core may increase (as observed in summer time today). Also, precipitation in Patagonia may increase again, suppressing dust mobilization and prompting vegetation to grow on previously dusty soil.

As illustrated in Figure 5, the rapid stepwise dust increases occurred very early during the deglaciation, i.e. when temperatures were still low and glacier extent in Patagonia still at its maximum. Therefore, a thermodynamic effect on

precipitation rate and washout of aeolian dust at that time is expected to be still small. However, at this time Na^+ concentrations in the ice core also started to decline, pointing to a reduction in sea ice and/or storminess in the Southern Ocean (Bigler et al., 2010; Wolff et al., 2006). Accordingly, we conclude that the strong change in dust mobilization and transport to the Antarctic ice sheet observed in our record at the beginning of the terminations is more likely connected to a rapid atmospheric reorganization at that time. This is also supported by the fact that many large Antarctic warming events show a similar fast dust response, with drops of 50% of the initial level or more within a few centuries (vertical arrows in Figure 4). There is no obvious threshold in temperature or sea-level that would provoke such fast changes in dust mobilization, especially since dust changes always lead changes in temperature. It would therefore appear that Southern Hemisphere atmospheric changes preceded the rise of temperature in the Southern Ocean during terminations and Antarctic warming events.

3.2.3 Distributions

We investigated the distribution of the dust flux during selected time periods using 25 year averages of the logarithmized and detrended $nssCa^{2+}$ data. For the Holocene very little LPD data exist (Fig. 1). Moreover, the CPH LPD data over the last 42 kyr were rescaled to the Bern LPD data, and hence do not allow for an independent estimate of the dust flux distribution. Accordingly, we only discuss the $nssCa^{2+}$ distributions over the entire 800,000 year record. Note

however that the overall glacial/interglacial change in the variability of the data discussed below is also seen in the LPD data as illustrated in Fig. 1. The distributions were separately plotted for the interglacials (Fig. 6a) and the glacials (Fig. 6b).

In all studied sections, the distributions of the logarithmic nssCa^{2+} fluxes are well fitted by a Gaussian distribution. This indicates that the fundamental processes governing dust uptake, transport to, and deposition in Antarctica were probably never fundamentally disturbed, and similar to modern conditions. In particular, extraordinary dust storm events that cannot be described by the background distribution did not occur during glacials, and are therefore not responsible for the very high glacial fluxes. However, there is a distinct difference in the width of the distributions between climatic optima and glacial maxima. Warm periods are characterized by a broad distribution, while cold periods have a markedly narrower one. MIS 16, that is thought to have been one of the coldest glacials in the past million years (Lisiecki and Raymo, 2005), shows the narrowest of all distributions, whereas the highest variability is featured during MIS 11, which was the longest interglacial.

The narrower glacial distribution agrees favourably with higher, but more steady wind speed in South America, when compared to interglacials. Once again, we can link this to the latitudinal shift or extension of the westerly wind belt in South America. As has been proposed in the last chapter, during cold times, intensive

westerly winds are found more to the north, whereas the relaxation of wind stress in the south allows regular cyclonic activity from the drake passage. This results in a higher and more regular dust enthralment. In conjunction with a longer atmospheric residence time due to a weaker hydrological cycle, these changes could explain the factor of 25 between glacial and interglacial dust flux (Lambert et al., 2008).

4. Conclusions

The Ca^{2+}, $nssCa^{2+}$ and insoluble particulate dust data from the EPICA Dome C ice core are presented at 1 cm depth resolution, corresponding to a formal sub-annual time resolution at the top and ~25 years at the bottom of the core.

The calcium to insoluble dust ratio varies by up to a factor of 6 between glacials and interglacials, with higher values during interglacials. The changes can be attributed mostly to variations in the Ca^{2+}/dust ratio of glacial and interglacial dust particles. These variations could be a result of the additional soluble Ca^{2+} leached by the more acidic atmosphere during warm times and/or from different Ca^{2+}/dust ratios of the dust sources during both time intervals.

Using the calcium, nss-calcium and insoluble dust records, a new dust flux dataset was created using Principal Component Analysis. The new record consists of the variability common to all three datasets and represents the best

high-resolution estimate for atmospheric dust flux variability during the past 800 kyr. Based on this dust flux record, the occurrence of Antarctic warming was investigated and the events identified during the past eight glacial periods. Such dust imprints of Antarctic warming events can be found during all glacial periods. They occur about 2-3 times every 10 kyr throughout the last 800,000 years. Southern Hemisphere millennial and centennial variability thus appears to have been a persistent feature of past glacial periods. The timing and leads and lags of dust with temperature, CO_2 and sea-level during glacial terminations were investigated. Dust usually reaches interglacial levels about 4 kyr before both temperature and CO_2. By that time CO_2 levels have never risen by more than 30 ppmv during the last 9 terminations. Iron fertilization by aerosol dust to the Southern Ocean can therefore only explain the smaller part of glacial-interglacial CO_2 changes. Dust flux also leads the major changes in sea-level, and there is no evidence for a consistent threshold value in sea-level that would impact on dust levels, although phase relationships on the independent marine and ice core age scales are highly uncertain. The abrupt changes seen in dust flux during terminations and Antarctic warming events within a few centuries suggest that changes in the hydrological cycle in the source region, possibly linked to changes in the latitudinal extension of the Westerlies, may have provoked the sudden drops in dust production and transport. Although not quite as rapid as the decadal atmospheric response to Dangaard-Oeschger events in the North Atlantic (NGRIP comm. members, 2004; Steffensen et al., 2008), the centennial jumps in dust flux in central Antarctica indicate quite drastic

reconfigurations in the wind regime also in the southern hemisphere, linked to climatic changes during the transitions and leading to substantial dust mobilization changes at that time. Their clear lead on temperature changes suggests that atmospheric reorganization in the Southern Hemisphere occurred before the Southern Ocean had warmed up significantly.

Both glacial and interglacial dust distribution are unimodal and can be well described by a log-normal distribution. Glacials display a narrower standard deviation than interglacials, which we interpret as reflecting the steadier atmospheric conditions in South America during glacial times. We conclude that the processes responsible for dust uptake and transport were not significantly altered from glacial to interglacial conditions. However, replenishment of dust supply, e.g. by glacial outwash, in parallel to higher mean wind speeds and reduced precipitation and vegetation can explain a largely increased glacial source strength in southern South America. Together with the larger atmospheric residence time connected to lower precipitation en route, this can explain the 25 times higher dust fluxes in Antarctica during the glacial.

Figures

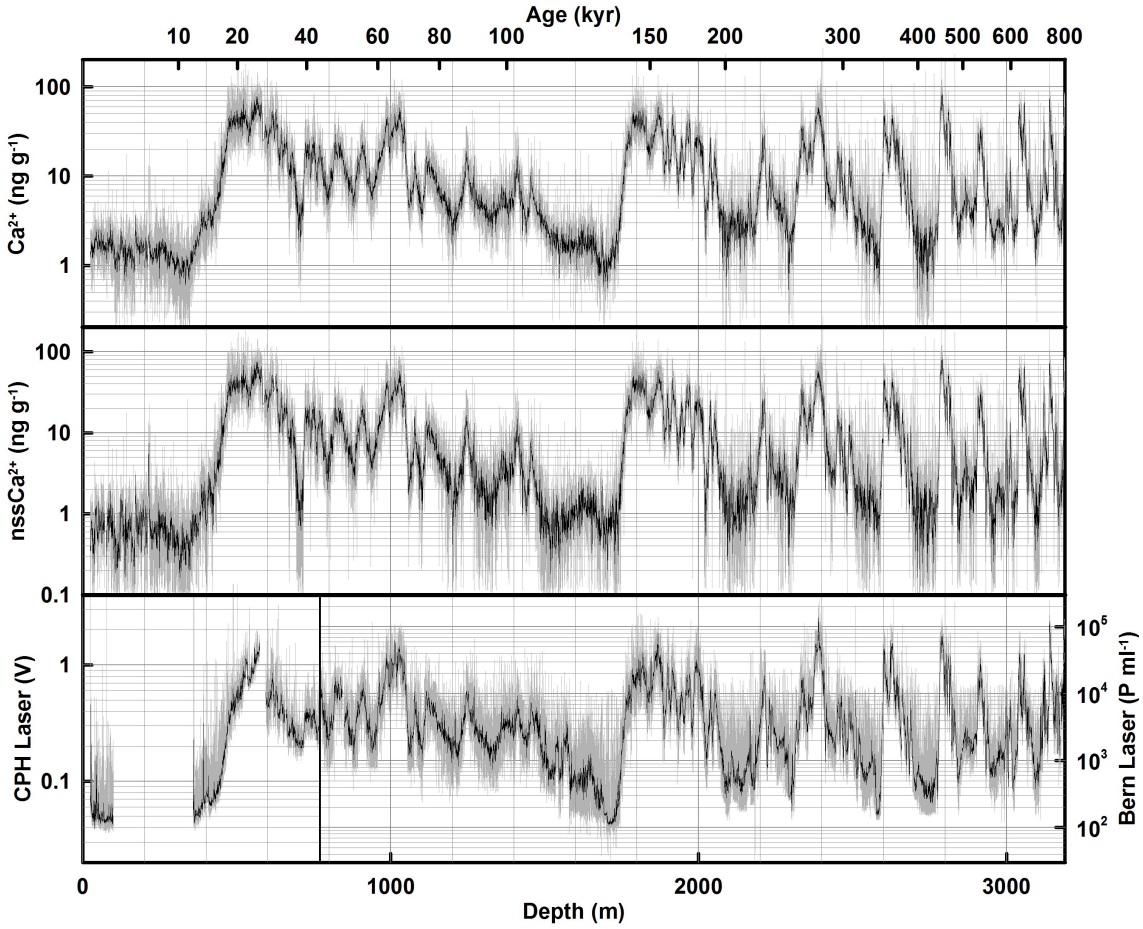

Figure 1: Calcium, non-sea-salt calcium, and dust data at 1 cm resolution (grey), overlain with 55 cm mean values (black) from EPICA Dome C CFA on the depth scale. The EDC3 time-scale in kyr is indicated on top. Dust was not measured between 100 and 358 m depth. Note that the CPH and Bern dust data have different y-axes.

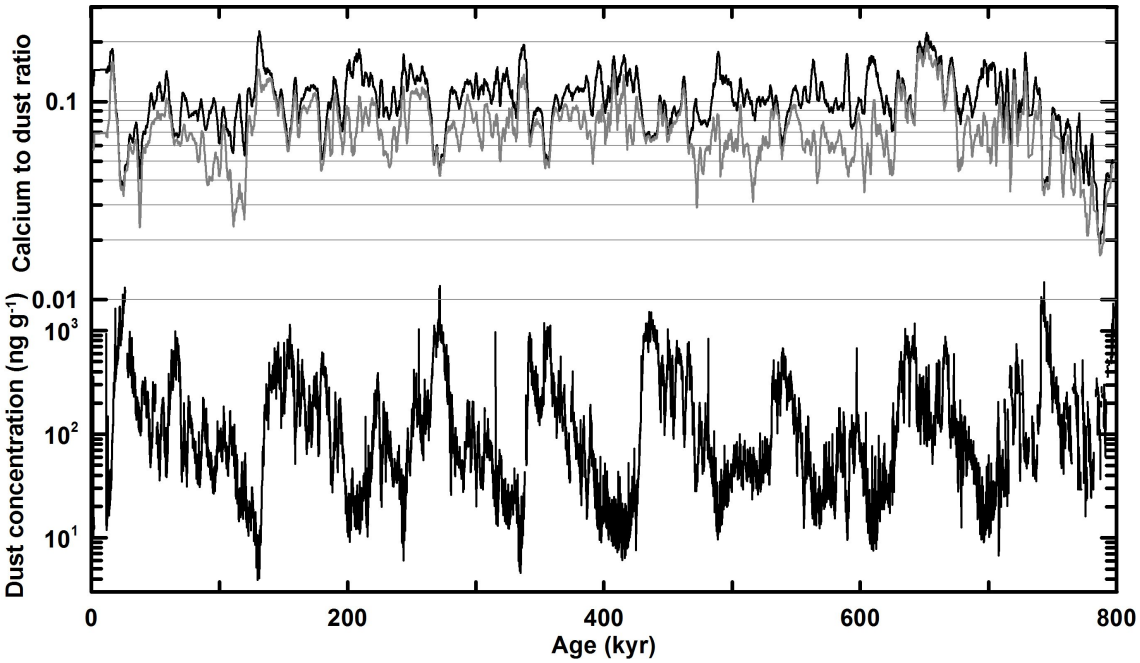

Figure 2: Insoluble dust concentrations in ng g^{-1} with ratio of Ca^{2+} and dust (in black), and $nssCa^{2+}$ and dust (in grey) concentrations, using 100 yr median values, on a logarithmic scale. Ratios have been smoothed by a 2500 year running average.

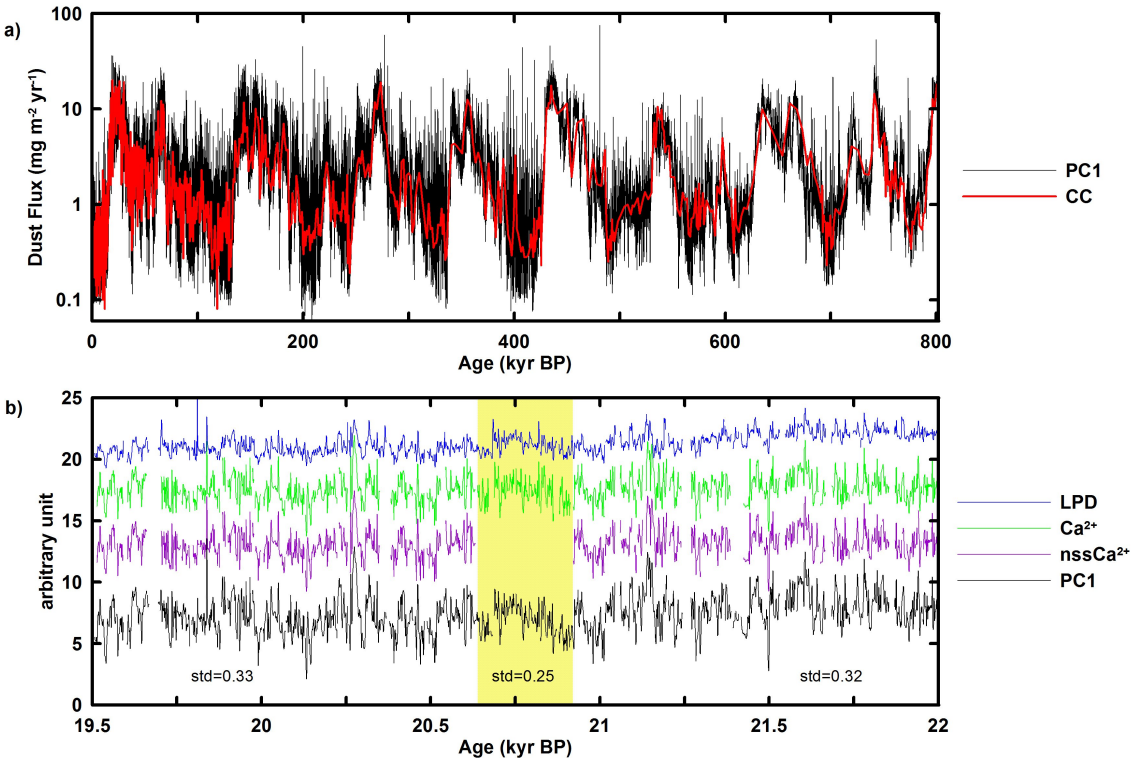

Figure 3: a) The first Principle Component (PC1) from the PCA (in black) has been calibrated with the Coulter Counter dust flux data (in red (Lambert et al., 2008)). b) Example section featuring Ca^{2+}, $nssCa^{2+}$, and particulate dust data and the first Principal Component. Only where gaps are present in all three original datasets does the PC1 also feature a gap.

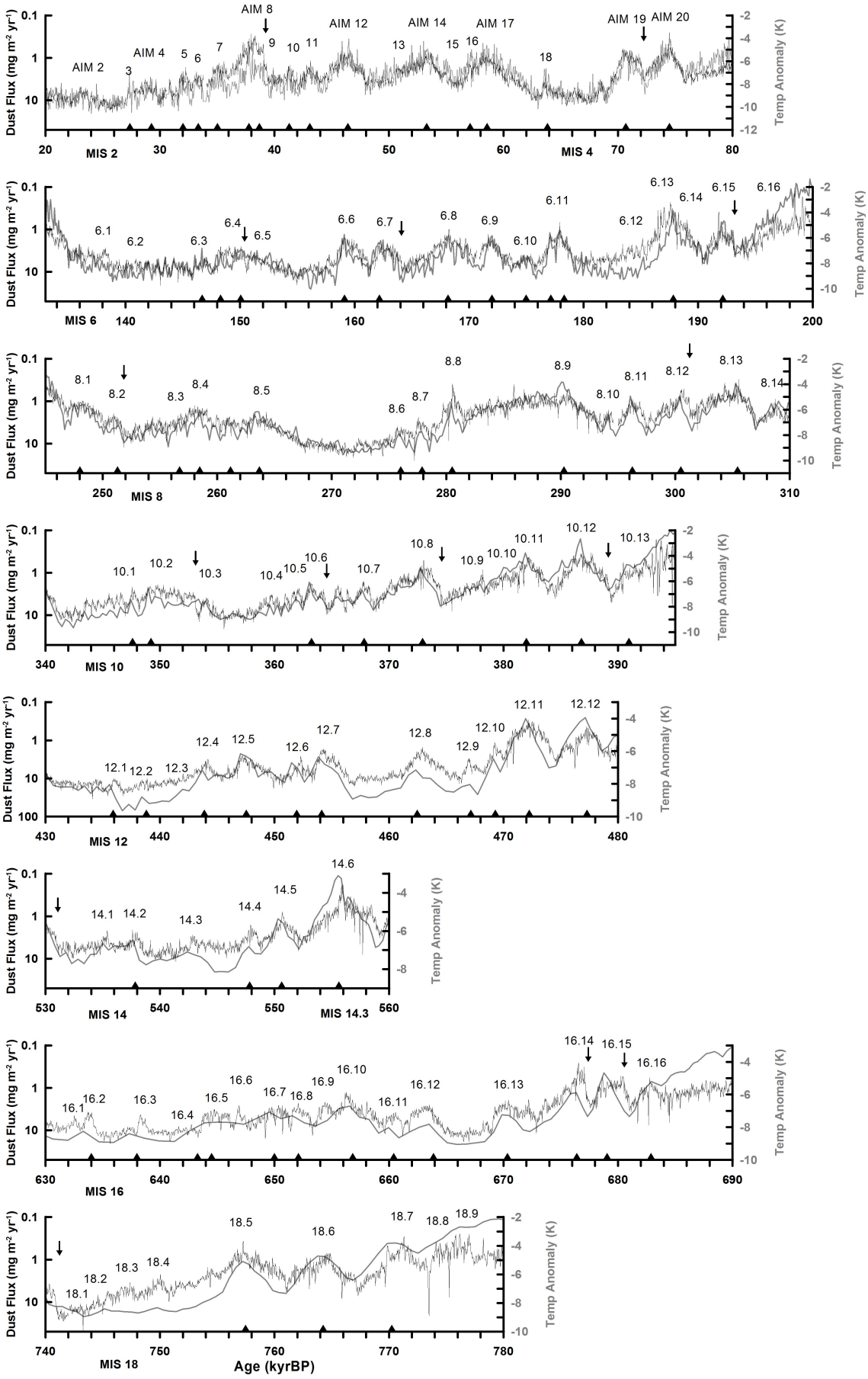
Dust Flux (mg m-2 yr-1)
Temp Anomaly (K)
AIM 2
AIM 4
AIM 8
AIM 12
AIM 14
AIM 17
AIM 19
AIM 20
MIS 2
MIS 4
MIS 6
MIS 8
MIS 10
MIS 12
MIS 14
MIS 14.3
MIS 16
MIS 18
Age (kyrBP)

Figure 4: 25 year mean dust flux data in black underlain with the EDC temperature data at original 55 cm depth resolution (Jouzel et al., 2007) back to 800 kyr BP. Antarctic Isotopic Maxima (AIM) are marked as identified in (EPICA comm. members, 2006). Vertical arrows mark the rapid dust flux jumps. The triangles mark the predicted occurrence of DO events based on the EDC δDeuterium data (Barker et al., 2011).

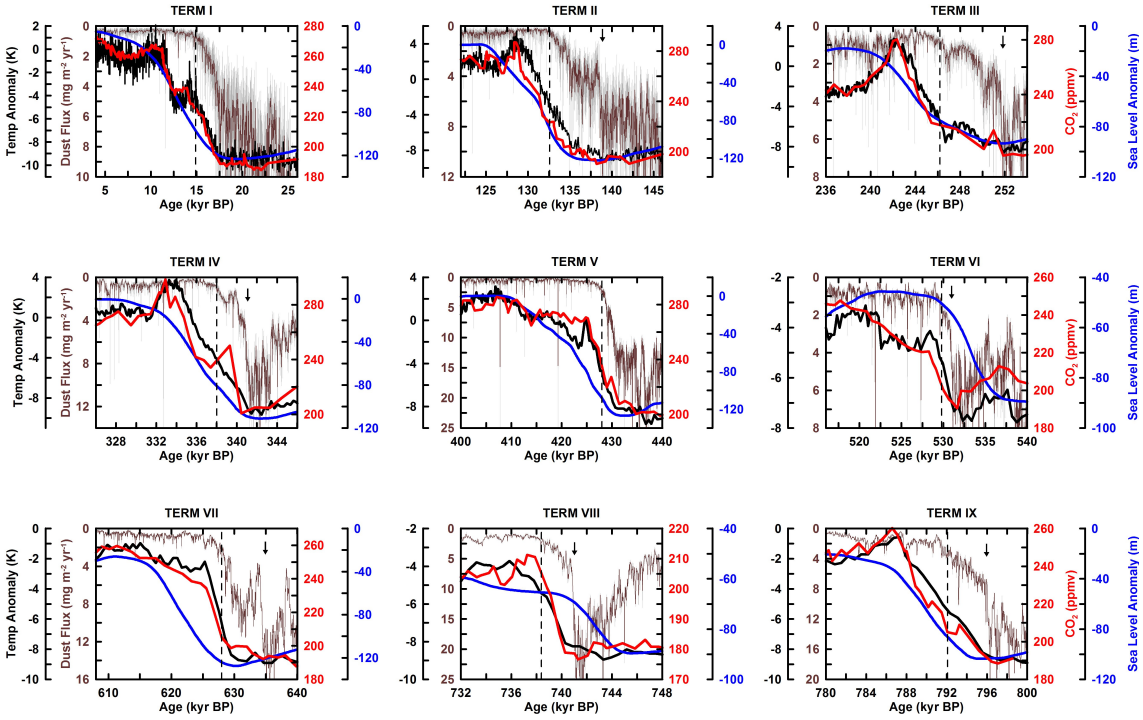

Figure 5: Evolution of dust flux (on an inverted axis at 1 cm resolution in grey overlaid with a 25 yr mean in brown), EDC temperature ((Jouzel et al., 2007) in black), CO_2 concentrations ((Lüthi et al., 2008) in red), and global sea-level ((Bintanja et al., 2005) in blue) during the past nine glacial terminations. The dashed line marks the time when dust flux reaches interglacial conditions. Vertical arrows mark the rapid dust jumps.

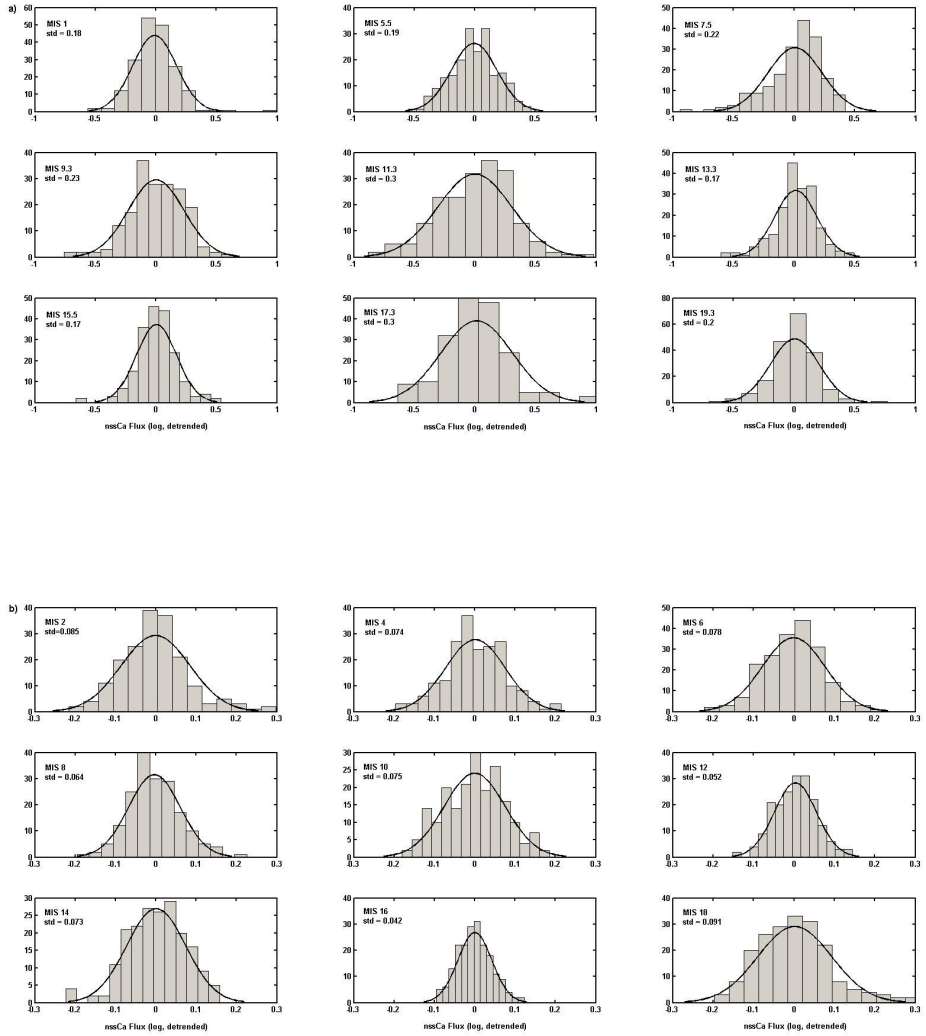

Figure 6: Distribution during 5 kyr sections of a) interglacials and b) glacials using detrended and logarithmized 25 year mean nssCa^{2+} data. The standard deviations shown are from the Gaussian fit.

References

Abdi, H. and Williams, L. J.: Principal component analysis, Wiley Interdisciplinary Reviews: Computational Statistics, 2(4), 433-459, doi:10.1002/wics.101, 2010.

Barker, S., Knorr, G., Edwards, R. L., Parrenin, F., Putnam, A. E., Skinner, L. C., Wolff, E. and Ziegler, M.: 800,000 Years of Abrupt Climate Variability., Science, 347, 0-5, doi:10.1126/science.1203580, 2011.

Bigler, M.: Hochaufloesende Spurenstoffmessungen an polaren Eisbohrkernen: Glazio-chemische und klimatische Prozessstudien, Ph. D. thesis, University of Bern, University of Bern., 2004.

Bigler, M., Röthlisberger, R., Lambert, F., Stocker, T. F. and Wagenbach, D.: Aerosol deposited in East Antarctica over the last glacial cycle: Detailed apportionment of continental and sea-salt contributions, Journal of Geophysical Research, 111(D8), 1-14, doi:10.1029/2005JD006469, 2006.

Bigler, M., Röthlisberger, R., Lambert, F., Wolff, E. W., Castellano, E., Udisti, R., Stocker, T. F. and Fischer, H.: Atmospheric decadal variability from high-resolution Dome C ice core records of aerosol constituents beyond the Last Interglacial, Quaternary Science Reviews, 29(1-2), 324-337, doi:10.1016/j.quascirev.2009.09.009, 2010.

Bintanja, R., van de Wal, R. S. W. and Oerlemans, J.: Modelled atmospheric temperatures and global sea levels over the past million years., Nature, 437(7055), 125-8, doi:10.1038/nature03975, 2005.

Blunier, T. and Brook, E. J.: Timing of millennial-scale climate change in Antarctica and Greenland during the last glacial period., Science, 291(5501), 109-12, doi:10.1126/science.291.5501.109, 2001.

Bopp, L.: Dust impact on marine biota and atmospheric CO 2 during glacial periods, Paleoceanography, 18(2), doi:10.1029/2002PA000810, 2003.

Bowen, H. J. M.: Environmental Chemistry of the Elements, Academic Press, London., 1979.

Delmonte, B., Andersson, P. S., Hansson, M., Schöberg, H., Petit, J. R., Basile-Doelsch, I. and Maggi, V.: Aeolian dust in East Antarctica (EPICA-Dome C and Vostok): Provenance during glacial ages over the last 800 kyr, Geophysical Research Letters, 35(7), 2-7, doi:10.1029/2008GL033382, 2008.

Delmonte, B., Andersson, P. S., Schöberg, H., Hansson, M., Petit, J. R., Delmas, R., Gaiero, D. M., Maggi, V. and Frezzotti, M.: Geographic provenance of aeolian dust in East Antarctica during Pleistocene glaciations: preliminary results from Talos Dome and comparison with East Antarctic and new Andean ice core data, Quaternary Science Reviews, 29(1-2), 256-264, doi:10.1016/j.quascirev.2009.05.010, 2010.

Delmonte, B., Basile-Doelsch, I., Petit, J.-R., Maggi, V., Revel-Rolland, M., Michard, A., Jagoutz, E. and Grousset, F.: Comparing the Epica and Vostok dust records during the last 220,000 years: stratigraphical correlation and provenance in glacial periods, Earth-Science Reviews, 66(1-2), 63-87, doi:10.1016/j.earscirev.2003.10.004, 2004.

Delmonte, B., Petit, J. R. and Maggi, V.: Glacial to Holocene implications of the new 27000-year dust record from the EPICA Dome C (East Antarctica) ice core, Climate Dynamics, 18(8), 647-660, doi:10.1007/s00382-001-0193-9, 2002.

EPICA comm. members: Eight glacial cycles from an Antarctic ice core., Nature, 429(6992), 623-8, doi:10.1038/nature02599, 2004.

EPICA comm. members: One-to-one coupling of glacial climate variability in Greenland and Antarctica, Nature, 444(7116), 195-198, doi:10.1038/nature05301 [online] Available from: http://www.nature.com/doifinder/10.1038/nature05301 (Accessed 11 July 2011), 2006.

Fischer, H., Fundel, F., Ruth, U., Twarloh, B., Wegner, A., Udisti, R., Becagli, S., Castellano, E., Morganti, A. and Severi, M.: Reconstruction of millennial changes in dust emission, transport and regional sea ice coverage using the deep EPICA ice cores from the Atlantic and Indian Ocean sector of Antarctica, Earth and Planetary Science Letters, 260(1-2), 340-354, doi:10.1016/j.epsl.2007.06.014, 2007a.

Fischer, H., Schmitt, J., Lüthi, D., Stocker, T. F., Tschumi, T., Parekh, P., Joos, F., Köhler, P., Völker, C., Gersonde, R., Barbante, C., et al.: The role of Southern Ocean processes in orbital and millennial CO2 variations – A synthesis, Quaternary Science Reviews, 29(1-2), 193-205, doi:10.1016/j.quascirev.2009.06.007, 2010.

Fischer, H., Siggaard-Andersen, M. L., Ruth, U., Röthlisberger, R. and Wolff, E. W.: Glacial / Interglacial changes in mineral dust and sea-salt records in polar ice cores: sources, transport, and deposition, Reviews of Geophysics, 45,

doi:10.1029/2005RG000192, 2007b.
Fuhrer, K., Wolff, E. W. and Johnsen, S. J.: Timescales for dust variability in the Greenland Ice Core Project(GRIP) ice core in the last 100, 000 years, Journal of Geophysical Research, 104(D24), 31043–31052, doi:10.1029/1999JD900929, 1999.
Gaiero, D. M.: Dust provenance in Antarctic ice during glacial periods: From where in southern South America?, Geophysical Research Letters, 34(17), 1-6, doi:10.1029/2007GL030520, 2007.
Jouzel, J., Masson-Delmotte, V., Cattani, O., Dreyfus, G., Falourd, S., Hoffmann, G., Minster, B., Nouet, J., Barnola, J. M., Chappellaz, J., Fischer, H., et al.: Orbital and millennial Antarctic climate variability over the past 800,000 years., Science, 317(5839), 793-6, doi:10.1126/science.1141038, 2007.
Kaufmann, P. R., Federer, U., Hutterli, M. a, Bigler, M., Schüpbach, S., Ruth, U., Schmitt, J. and Stocker, T. F.: An improved continuous flow analysis system for high-resolution field measurements on ice cores, Environmental science & technology, 42(21), 8044-50, doi:10.1021/es8007722, 2008.
Köhler, P. and Fischer, H.: Simulating low frequency changes in atmospheric CO2 during the last 740 000 years, Climate of the Past, 2(2), 57-78, doi:10.5194/cp-2-57-2006, 2006.
Köhler, P., Fischer, H., Munhoven, G. and Zeebe, R. E.: Quantitative interpretation of atmospheric carbon records over the last glacial termination, Global Biogeochemical Cycles, 19(4), doi:10.1029/2004GB002345, 2005.
Lambert, F., Delmonte, B., Petit, J. R., Bigler, M., Kaufmann, P. R., Hutterli, M. a, Stocker, T. F., Ruth, U., Steffensen, J. P. and Maggi, V.: Dust-climate couplings over the past 800,000 years from the EPICA Dome C ice core., Nature, 452(7187), 616-9, doi:10.1038/nature06763, 2008.
Lamy, F., Kilian, R., Arz, H. W., Francois, J.-P., Kaiser, J., Prange, M. and Steinke, T.: Holocene changes in the position and intensity of the southern westerly wind belt, Nature Geoscience, 3(10), 695-699, doi:10.1038/ngeo959, 2010.
LeGrand, P. and Alverson, K.: Variations in atmospheric CO 2 during glacial cycles from an inverse ocean modeling perspective, Paleoceanography, 16(6), 604, doi:10.1029/2000PA000553, 2001.
Legrand, M. and Mayewski, P.: Glaciochemistry of polar ice cores: A review, Reviews of Geophysics, 35(3), 219, doi:10.1029/96RG03527, 1997.

Lisiecki, L. E. and Raymo, M. E.: A Pliocene-Pleistocene stack of 57 globally distributed benthic δ 18 O records, Paleoceanography, 20(1), 1-17, doi:10.1029/2004PA001071, 2005.

Loulergue, L., Schilt, A., Spahni, R., Masson-Delmotte, V., Blunier, T., Lemieux, B., Barnola, J.-M., Raynaud, D., Stocker, T. F. and Chappellaz, J.: Orbital and millennial-scale features of atmospheric CH4 over the past 800,000 years., Nature, 453(7193), 383-6, doi:10.1038/nature06950 [online] Available from: http://www.ncbi.nlm.nih.gov/pubmed/18480822 (Accessed 20 July 2011), 2008.

Lässig, J. L., Cogliati, M. G., Bastanski, M. A. and Palese, C.: Wind characteristics in Neuquen , North Patagonia , Argentina, Journal of Wind Engineering and Industrial Aerodynamics, 79, 183-199, doi:10.1016/S0167-6105(98)00110-X, 1999.

Lüthi, D., Le Floch, M., Bereiter, B., Blunier, T., Barnola, J.-M., Siegenthaler, U., Raynaud, D., Jouzel, J., Fischer, H., Kawamura, K. and Stocker, T. F.: High-resolution carbon dioxide concentration record 650,000-800,000 years before present., Nature, 453(7193), 379-82, doi:10.1038/nature06949, 2008.

Maher, B. a., Prospero, J. M., Mackie, D., Gaiero, D., Hesse, P. P. and Balkanski, Y.: Global connections between aeolian dust, climate and ocean biogeochemistry at the present day and at the last glacial maximum, Earth-Science Reviews, 99(1-2), 61-97, doi:10.1016/j.earscirev.2009.12.001, 2010.

Mahowald, N. M., Muhs, D. R., Levis, S., Rasch, P. J., Yoshioka, M., Zender, C. S. and Luo, C.: Change in atmospheric mineral aerosols in response to climate: Last glacial period, preindustrial, modern, and doubled carbon dioxide climates, Journal of Geophysical Research, 111(D10), doi:10.1029/2005JD006653, 2006a.

Mahowald, N. M., Yoshioka, M., Collins, W. D., Conley, A. J., Fillmore, D. W. and Coleman, D. B.: Climate response and radiative forcing from mineral aerosols during the last glacial maximum, pre-industrial, current and doubled-carbon dioxide climates, Geophysical Research Letters, 33(20), 2-5, doi:10.1029/2006GL026126, 2006b.

Martin, J. H., Gordon, R. M. and Fitzwater, S. E.: Iron in Antarctic waters, Nature, 345(6271), 156-158, doi:10.1038/345156a0, 1990.

Martin, J. H., Gordon, R. M. and Fitzwater, S. E.: The Case for Iron, Limnology and Oceanography, 36(8), 1793-1802, 1991.

Martrat, B., Grimalt, J. O., Shackleton, N. J., de Abreu, L., Hutterli, M. A. and

Stocker, T. F.: Four climate cycles of recurring deep and surface water destabilizations on the Iberian margin., Science (New York, N.Y.), 317(5837), 502-7, doi:10.1126/science.1139994, 2007.
Martínez-Garcia, A., Rosell-Melé, A., Jaccard, S. L., Geibert, W., Sigman, D. M. and Haug, G. H.: Southern Ocean dust–climate coupling over the past four million years, Nature, 476(7360), 312-315, doi:10.1038/nature10310, 2011.
Mayewski, P. A., Meeker, L. D., Whitlow, S., Twickler, M. S., Morrison, M. C., Bloomfield, P., Bond, G. C., Alley, R. B., Gow, A. J., Meese, D. A., Grootes, P. M., et al.: Changes in Atmospheric Circulation and Ocean Ice Cover over the North Atlantic During the Last 41,000 Years., Science, 263(5154), 1747-51, doi:10.1126/science.263.5154.1747, 1994.
Miller, R. L. and Tegen, I.: Climate Response to Soil Dust Aerosols, Journal of Climate, 11(12), 3247-3267, doi:10.1175/1520-0442(1998)011<3247:CRTSDA>2.0.CO;2, 1998.
NGRIP comm. members: High-resolution record of Northern Hemisphere climate extending into the last interglacial period., Nature, 431(7005), 147-51, doi:10.1038/nature02805, 2004.
Parekh, P., Joos, F. and Müller, S. A.: A modeling assessment of the interplay between aeolian iron fluxes and iron-binding ligands in controlling carbon dioxide fluctuations during Antarctic warm events, Paleoceanography, 23(4), PA4202, doi:10.1029/2007PA001531, 2008.
Rankin, A. M., Auld, V. and Wolff, E. W.: Frost flowers as a source of fractionated sea salt aerosol in the polar regions, Geophysical Research Letters, 27(21), 3469, doi:10.1029/2000GL011771, 2000.
Revel-Rolland, M., Dedeckker, P., Delmonte, B., Hesse, P., Magee, J., Basiledoelsch, I., Grousset, F. and Bosch, D.: Eastern Australia: A possible source of dust in East Antarctica interglacial ice, Earth and Planetary Science Letters, 249(1-2), 1-13, doi:10.1016/j.epsl.2006.06.028, 2006.
Ridgwell, A. J.: Implications of the glacial CO 2 “iron hypothesis” for Quaternary climate change, Geochemistry Geophysics Geosystems, 4(9), 1-10, doi:10.1029/2003GC000563, 2003.
Ruth, U., Barbante, C., Bigler, M., Delmonte, B., Fischer, H., Gabrielli, P., Gaspari, V., Kaufmann, P., Lambert, F., Maggi, V., Marino, F., et al.: Proxies and measurement techniques for mineral dust in Antarctic ice cores, Environmental Science & Technology, 42(15), 5675-81, doi:10.1021/es703078z, 2008.

Ruth, U., Wagenbach, D., Bigler, M., Steffensen, J. P., Röthlisberger, R. and Miller, H.: High resolution microparticle profiles at NGRIP: case studies of the calcium-dust relationship, Annals of Glaciology, 35, 237-242, 2002.

Ruth, U., Wagenbach, D., Steffensen, J. P. and Bigler, M.: Continuous record of microparticle concentration and size distribution in the central Greenland NGRIP ice core during the last glacial period, Journal of Geophysical Research, 108(D3), 1-12, doi:10.1029/2002JD002376, 2003.

Röthlisberger, R., Bigler, M., Hutterli, M., Sommer, S., Stauffer, B., Junghans, H. G. and Wagenbach, D.: Technique for continuous high-resolution analysis of trace substances in firn and ice cores, Environ. Sci. Technol, 34(2), 338–342, doi:10.1021/es9907055, 2000.

Röthlisberger, R., Bigler, M., Wolff, E. W., Joos, F., Monnin, E. and Hutterli, M. A.: Ice core evidence for the extent of past atmospheric CO 2 change due to iron fertilisation, Geophysical Research Letters, 31(16), 2-5, doi:10.1029/2004GL020338, 2004.

Röthlisberger, R., Mulvaney, R., Wolff, E. W., Hutterli, M. A., Bigler, M., Sommer, S. and Jouzel, J.: Dust and sea salt variability in central East Antarctica (Dome C) over the last 45 kyrs and its implications for southern high-latitude climate, Geophysical Research Letters, 29(20), 1-5, doi:10.1029/2002GL015186, 2002.

Sassen, K., Demott, P. J., Prospero, J. M. and Poellot, M. R.: Saharan dust storms and indirect aerosol effects on clouds : CRYSTAL-FACE results, Geophysical Research Letters, 30(12), 1-4, doi:10.1029/2003GL017371, 2003.

Schwartz, S. E.: The whitehouse effect-shortwave radiative forcing of climate by anthropogenic aerosols: an overview, J. Aerosol. Sci, 27, 359-382, doi:10.1016/0021-8502(95)00533-1, 1996.

Sigman, D. M., Hain, M. P. and Haug, G. H.: The polar ocean and glacial cycles in atmospheric CO(2) concentration., Nature, 466(7302), 47-55, doi:10.1038/nature09149, 2010.

Steffensen, J. P., Andersen, K. K., Bigler, M., Clausen, H. B., Dahl-Jensen, D., Fischer, H., Goto-Azuma, K., Hansson, M., Johnsen, S. J., Jouzel, J., Masson-Delmotte, V., et al.: High-resolution Greenland ice core data show abrupt climate change happens in few years., Science, 321(5889), 680-4, doi:10.1126/science.1157707, 2008.

Stocker, T. F. and Johnsen, S. J.: A minimum thermodynamic model for the bipolar seesaw, Paleoceanography, 18(4), 1087-1089,

doi:10.1029/2003PA000920, 2003.
Tegen, I.: Modeling the mineral dust aerosol cycle in the climate system, Quaternary Science Reviews, 22(18-19), 1821-1834, doi:10.1016/S0277-3791(03)00163-X, 2003.
Tegen, I., Lacis, A. and Fung, I.: The influence on climate forcing of mineral aerosols from disturbed soils, Nature, 380, 419-422, doi:10.1038/380419a0, 1996.
Watson, A. J. and Naveira Garabato, A. C.: The role of Southern Ocean mixing and upwelling in glacial-interglacial atmospheric CO2 change, Tellus Series B Chemical And Physical Meteorology, 58(1), 73-87, doi:10.1111/j.1600-0889.2005.00167.x, 2006.
Watson, A. J., Bakker, D. C., Ridgwell, A. J., Boyd, P. W. and Law, C. S.: Effect of iron supply on Southern Ocean CO2 uptake and implications for glacial atmospheric CO2., Nature, 407(6805), 730-3, doi:10.1038/35037561, 2000.
Winckler, G. and Fischer, H.: 30,000 years of cosmic dust in Antarctic ice., Science, 313(5786), 491, doi:10.1126/science.1127469, 2006.
Wolff, E. W., Fischer, H., Fundel, F., Ruth, U., Twarloh, B., Littot, G. C., Mulvaney, R., Röthlisberger, R., de Angelis, M., Boutron, C. F., Hansson, M., et al.: Southern Ocean sea-ice extent, productivity and iron flux over the past eight glacial cycles., Nature, 440(7083), 491-6, doi:10.1038/nature04614, 2006.
Wolff, E., Fischer, H. and Röthlisberger, R.: Glacial terminations as southern warmings without northern control, Nature Geoscience, 2(March), 206-209, doi:10.1038/NGEO442, 2009.

B. The role of mineral dust aerosols in polar amplification

Mineral dust particles in the air both absorb and scatter incoming shortwave and outgoing longwave radiation[1]. They also act as condensation nuclei for ice and water droplets, thus affecting the climate indirectly[11]. Modern atmospheric dust concentrations can be derived from satellite measurements in certain areas, but only dust modeling studies have provided global estimates[3,4,12]. Information on dust deposition in the past can be obtained from climatic archives[13]. In turn, dust models can be tuned to match the observed depositions and provide an estimate for present and past atmospheric concentrations[4,5]. Global dust deposition at the LGM is thought to have been higher by a factor of 2-4 than during the Holocene[4,5,13,14]. While the optical properties of desert dust are uncertain, surface RF due to dust aerosols has been estimated in modeling studies at -0.2 to -1.2 and -0.43 to -3.2 Wm^{-2} for Holocene and LGM conditions, respectively[5–7].

In this work we propose an alternate way to estimate atmospheric dust loads during Holocene and LGM conditions by using observations to constrain our

dust concentration changes, with some information from the models. We then use these observations derived estimates to calculate dust-induced RF. Previous papers looking at the change in last glacial maximum versus current climate were based on model studies, with some attention to observations[4,6,7,12]. Model studies of dust have many sources of uncertainties, from the source areas, source strengths, transport pathways and deposition uncertainties. Here, we use only the relationship between the vertical profile and the deposition from the model. This reduces our dependency on the models and thus, potentially, our uncertainties. We use two different dust model studies to ascertain our uncertainties: the Community Atmospheric Model 3 coupled with the Climate Community System Model 3[4] (hereafter CCSM), as well as Tokyo University's SPRINTARS aerosol model coupled with the Model for Interdisciplinary Research On Climate[5] (hereafter MIROC) provide two different simulations of the dust cycle in both Holocene and LGM conditions.

The new DIRTMAP 3 database[14] increases the number of known dust deposition sites during both Holocene and LGM conditions by a factor of 3 compared to the previous dataset[13]. This data, combined with additional new

dust deposition measurements (table T1, suppl. mat.) was interpolated to a global dust deposition grid using a kriging algorithm. Surface concentrations were calculated by dividing the dry fraction of the deposition flux by the dry deposition velocity. The dry deposition fraction and velocity differ for both models and result in two slightly different surface concentration datasets. Method and uncertainties are discussed in the supplementary information. The reconstructions of surface dust concentrations based on CCSM and MIROC deposition data are compared in figure 1 to the surface concentrations from each model. Maximum and minimum values are similar in the reconstructions and the models. However, dust loads appear more zonally distributed in the reconstructions. This feature is highlighted in table 1a where the global and zonal median of surface dust concentrations are displayed. Dust concentrations are approximately log-normally distributed (fig. S2), we therefore use the median as a more representative indicator of globally or zonally distributed dust load than the average. Global median surface dust concentrations are estimated at 1.4 to 5.2 μg m^{-3} and 2.9 to 13.6 μg m^{-3} for Holocene and LGM conditions, respectively. This is higher than the model values and reflects the wider distribution of dust load estimates compared to the source peaks in the

models. Especially in high southern latitudes, the reconstruction appears to perform well with higher details than in the models, possibly reflecting small sources that are not included in the models. On the other hand, the lack of data in South America and Australia leads to an underestimation of these areas in the reconstruction compared to the models.

RF due to the reconstructed dust loads was estimated by comparing reconstruction zonal medians with each model's zonal direct shortwave (SW) + longwave (LW) RF to surface dust concentration relationship (fig. S3-S6). This rescaling is justified because direct RF evolves largely linearly with dust concentrations. Due to generally higher dust loads, the RF in the reconstructions tend to be higher than in their respective models. Table 1b summarizes the findings in latitudinal bands. The global average of direct RF (SW+LW) at the surface is estimated at -0.2 to -0.5 Wm^{-2} and -0.5 to -1.9 Wm^{-2} during Holocene and LGM conditions, respectively. The global averages are quite close to the model values, although some zonal differences are present.

The largest relative changes in dust concentrations and RF happen at high

latitudes. A disproportionate response to climate change in high latitudes is not confined to dust loads, but is also a feature of temperature response. Although LGM global and equatorial temperature were around 3 to 4 K colder than during the Holocene[15–17], this difference was much larger (8-17 degrees) at the poles[18–20], and we call this effect polar amplification (fig. 2). Polar amplification has been subjected to ample scrutiny in the context of rising temperature in the close future[21,22]. The mechanisms of this effect are still unclear, and climate models have consistently underestimated polar temperature amplification at the LGM[19]. The temperature profiles in figure 2 show the amplification factor as the difference to local average Holocene temperature divided by the global temperature change between Holocene and LGM. LGM to Holocene changes were double and quadruple the global average in Antarctica and Greenland, respectively. The LGM to Holocene radiative perturbation in high latitudes due to extended ice sheets has been estimated at -20 Wm^{-2} [7]. In comparison, the global effect of reduced CO_2 concentrations is believed to be -2.8 Wm^{-2} [23]. The dust data in figure 2 show the dust polar amplification as the local ratio to average Holocene concentrations divided by the global Holocene to LGM dust load change. As with temperature, the background dust load in low latitudes

agrees well with the estimated global average change. However, the change in dust depositions at the poles was one order of magnitude larger than the global average. It is plausible that the much higher atmospheric dust concentrations during the LGM had a significant impact on polar climate and may have contributed to the polar amplification phenomenon.

To investigate in detail the changes in polar regions, two sites were chosen over both the Greenland and the Antarctic ice sheet (table T2), far away from potential source areas. A remote site in the central Equatorial Pacific provides a low latitude comparison over a low albedo surface. At each location, average Holocene and LGM (defined as the time period from 8 kyr BP to 2 kyr BP and from 26 kyr BP to 19 kyr BP, respectively) dust flux levels were deduced from ice core or marine sediment data. These average flux levels can be considered as originating from polar background atmospheric dust loads. The uncertainty in ice core dust flux, as well as in the Thorium normalized marine sediment data, is relatively well constrained at under 30%[9,10,18]. Surface concentrations were reconstructed using the method discussed above (see suppl. mat.). Vertical dust concentration profiles were derived by scaling each model's profile to the

reconstructed surface concentrations.

Dust deposition is highest during spring and summer in polar areas, which coincides with peak mobilization in dust source areas[24–26]. According to recent modeling results, although dust deposition may be dominated by a few events close to the source, deposition at remote areas is more evenly distributed in time[27]. We can therefore assume that deposition at the poles was not due to single events, but spread out over time. However, since it is difficult to estimate how much dust gets deposited during spring and summer compared to the annual total, we consider two cases, bracketing the range of possible distribution. In the minimum scenario (MIN), dust deposition is evenly distributed during the year, while in the maximum scenario (MAX), all the dust is deposited during spring and summer. In both cases, dust-induced direct short-wave RF is only in effect during the polar summer.

Figure 3 shows the Greenland and Antarctic direct short-wave radiative forcing at the surface for both scenarios calculated with a one-dimensional rapid radiative transfer model[28]. In Holocene conditions, the low dust concentrations

at the poles result in low surface RF values in Greenland and Antarctica. Depending on model parameters and scenarios, the dust-induced surface RF in the central Pacific varies between -0.5 and -3.5 Wm^{-2} and -1 to -3 Wm^{-2} in Holocene and LGM condition, respectively. This is in agreement with the general results shown in table 1b. Unlike the zonal averages in the models and the global reconstructions, the RF from the detailed reconstructed LGM dust concentrations over ice shields shows an important effect due to atmospheric dust. Although both reconstructions differ in absolute values due to model differences in dry deposition velocity and vertical profile, they both feature a significant cooling at the surface. In Greenland, there is a -2.9 to -5.9 Wm^{-2} surface cooling (averaging the MAX and MIN values for each model), which corresponds to about double the effect due to lowered CO_2 concentrations at the LGM during polar summer, or a similar effect to CO_2 when considering yearly average values. In Antarctica, the surface cooling is still sizable at -0.9 to -1.8 Wm^{-2}. Long-wave forcing will slightly reduce these values. However, it is difficult to quantify this effect, as it is strongly weakened by cloud cover, and thus also dependent on the indirect effect of dust (see suppl. mat).

The SW RF is negative all along the air column over low albedo surfaces (fig, S7). However, as surface albedo increases, the RF curve is laterally shifted towards positive values. In polar areas, the RF is negative at the surface, but becomes positive in the higher atmosphere (fig. S7). In LGM conditions, this opposite warming and cooling in the high and low atmosphere would have increased atmospheric stability and therefore amplified surface cooling by preventing heat exchanges between near surface air and the free atmosphere. Furthermore, the cooling at the surface would have slowed down the melting of sea-ice and snow during spring and summer, thus keeping the albedo higher and inhibiting the warming of the polar region. Atmospheric dust aerosols may therefore have acted as a positive reinforcement in the polar cooling amplification during the LGM.

Our results suggest that the radiative impact of atmospheric dust aerosols during the LGM could have been underestimated, especially in polar areas. The detailed parameterization of aerosol RF could help models to recapture the full effect of the polar amplification and temperature distribution in different climates. Over the 20th century, the limited paleorecords suggest a doubling of desert dust[29], part of which may be due to natural and anthropogenic climate change

and partly due to land use change. In the future, droughts and land aridity are projected to increase[30], although carbon dioxide fertilization may partly offset some of these increases in desert dust source area[31]. It appears likely that desert dust sources may continue to increase in the future. Whether these will have similar polar amplification feedbacks as in the last glacial maximum is an important poorly understood problem.

Tables

a) Median surface concentrations (µg m^{-3})

Latitude	Reconstructions						Models					
band (°N)	CCSM(HOL)	CCSM(LGM)	Ratio LGM/HOL	MIROC(HOL)	MIROC(LGM)	Ratio LGM/HOL	CCSM(HOL)	CCSM(LGM)	Ratio LGM/HOL	MIROC(HOL)	MIROC(LGM)	Ratio LGM/HOL
60 to 90	0.53	8.7	16.42	0.02	1.32	55.00	0.24	4.71	19.63	0.016	0.046	2.99
30 to 60	6	40.35	6.73	4.82	19.75	4.10	4.03	29.88	7.41	0.31	0.54	1.72
0 to 30	25.54	36.28	1.42	14.57	21.75	1.49	9.34	13.77	1.47	3.42	6.57	1.92
0 to -30	20.78	24.1	1.16	2.76	4.29	1.55	2.26	3.97	1.76	0.30	0.38	1.25
-30 to -60	3.55	6.01	1.69	0.41	0.46	1.12	0.26	1.2	4.62	0.01	0.01	0.59
-60 to -90	0.16	0.46	2.88	0.0064	0.0314	4.91	0.0067	0.065	9.70	0.0007	0.0007	0.96
Global	5.2	13.58	2.61	1.37	2.93	2.14	0.78	4.48	5.74	0.1	0.1208	1.23

b) Direct radiative forcing SW+LW (W m^{-2})

Latitude	Reconstructions						Models					
band (°N)	CCSM(HOL)	CCSM(LGM)	LGM-HOL	MIROC(HOL)	MIROC(LGM)	LGM-HOL	CCSM(HOL)	CCSM(LGM)	LGM-HOL	MIROC(HOL)	MIROC(LGM)	LGM-HOL
60 to 90	-0.1	-0.5	-0.40	-0.02	N/A	N/A	-0.04	-0.78	-0.74	-0.02	-0.21	-0.19
30 to 60	-0.58	-3	-2.42	-0.4	-1.5	-1.10	-0.48	-2.83	-2.35	-0.23	-0.58	-0.35
0 to 30	-2.5	-5.2	-2.70	-0.7	-1.2	-0.50	-1.23	-2.35	-1.12	-0.5	-1.1	-0.60
0 to -30	-0.05	-2	-1.95	-0.21	-0.3	-0.09	-0.16	-0.72	-0.56	-0.08	-0.12	-0.04
-30 to -60	-0.03	-0.78	-0.75	-0.08	-0.07	0.01	-0.01	-0.81	-0.80	-0.04	-0.01	0.03
-60 to -90	N/A	-0.01	N/A	N/A	N/A	N/A	-0.0006	-0.002	-0.0014	0.0034	0.0025	-0.0009
Global*	-0.54	-1.92	-1.37	-0.24	-0.51	-0.28	-0.44	-1.5	-1.06	-0.2	-0.43	-0.23

Table 1: a) Comparison of reconstructed Holocene and LGM zonal median surface dust concentrations with model results[4,5]. b) Holocene and LGM zonally averaged direct radiative forcing (short-wave + long-wave) from reconstructed and modeled[5,6] dust concentrations.

* The reconstructed global RF were calculated by assuming that the missing polar values were negligible compared to the mid- and low latitudes RF. For the averaging they were set to zero.

Figures:

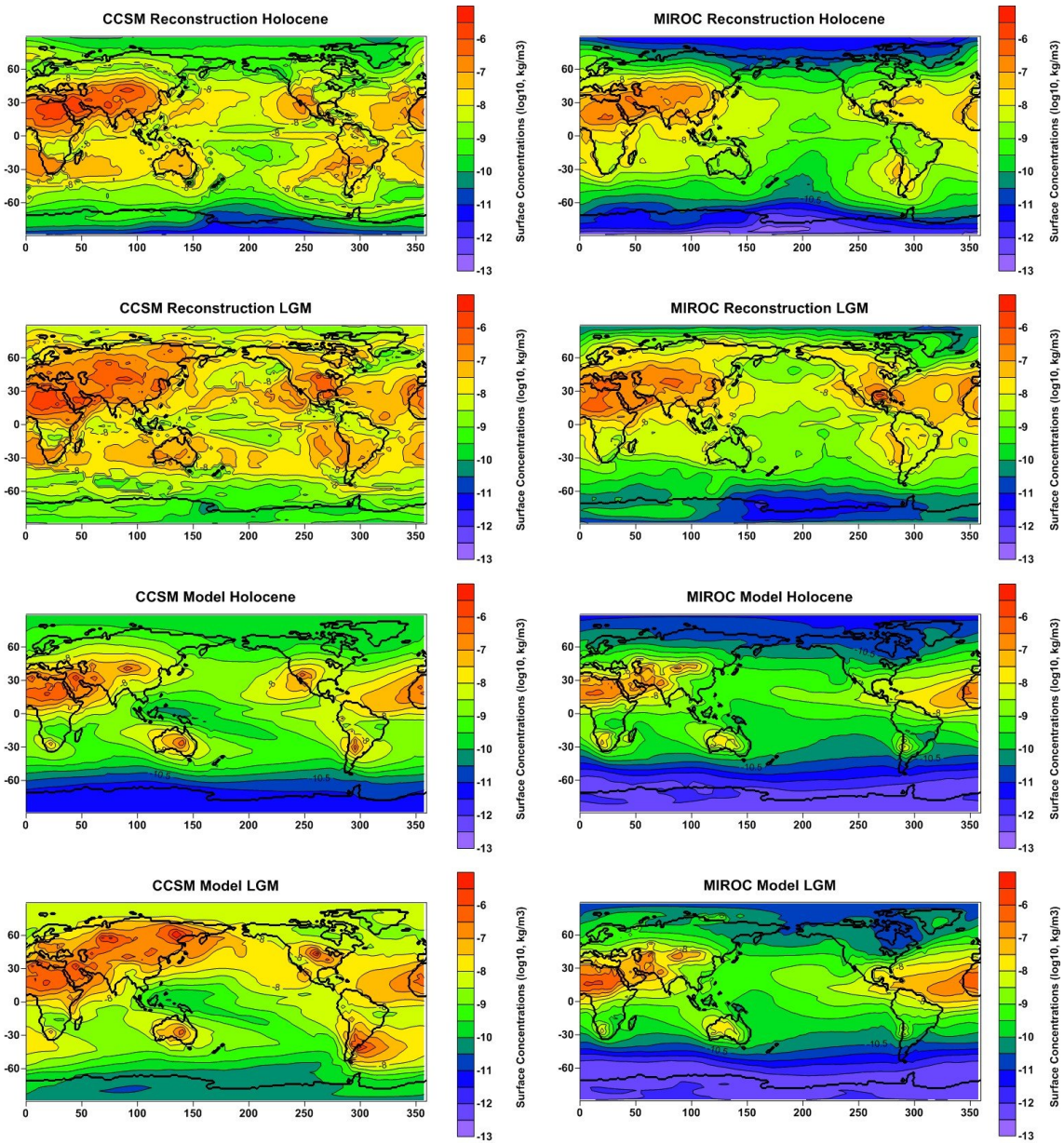

Fig. 1: Comparison of the surface concentrations in the CCSM and MIROC reconstruction and in the models[4,5]. The color bar marks the surface concentrations in logarithms of ten.

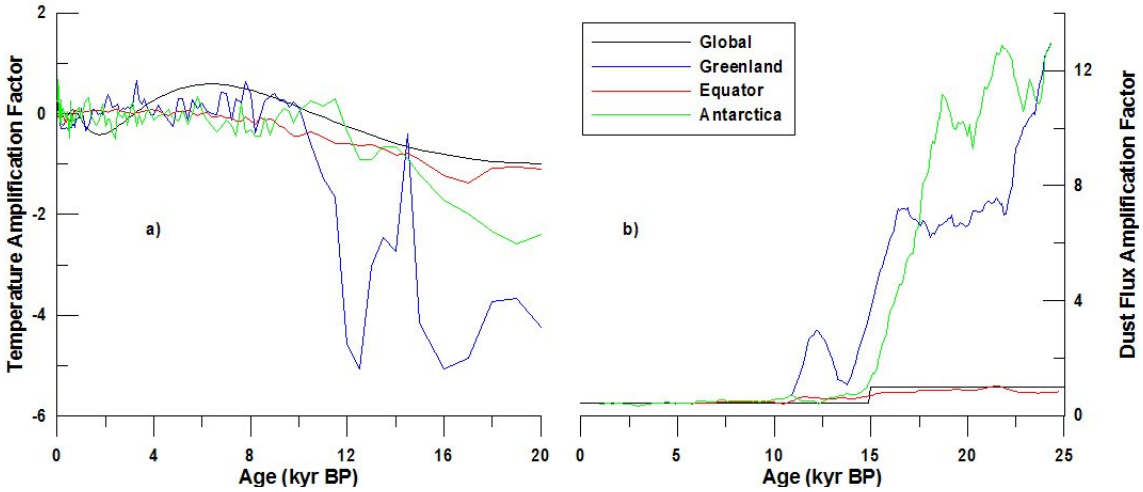

Fig. 2: a) Amplification of the temperature signal at the LGM. The Amplification A(t) is defined by A(t) = (T(t) - T(Holocene average)) / 3.4K. The global average change of -3.4K between Holocene and LGM corresponds to a factor of -1. The GISP2[20] and Dome C[18] temperature records are taken as representative for Greenland and Antarctic temperature changes, respectively. A marine sediment core from tropical Africa[17] shows temperature variations at the Equator, while a multi-proxy reconstruction[15] provides the global temperature changes. b) Amplification of dust concentrations at the LGM. The Amplification is defined as A(t) = (Conc(t) / Conc(Holocene average)) / 2.2. The global average dust load increased by a factor of 2.2 and corresponds to an amplification factor of 1. The NGRIP[9] and Dome C[8] dust records represent Greenland and Antarctic dust load

variations, respectively. A marine sediment core from the central equatorial Pacific[10] gives an equatorial reference, while the global dust load change was taken from the DIRTMAP[13] dataset.

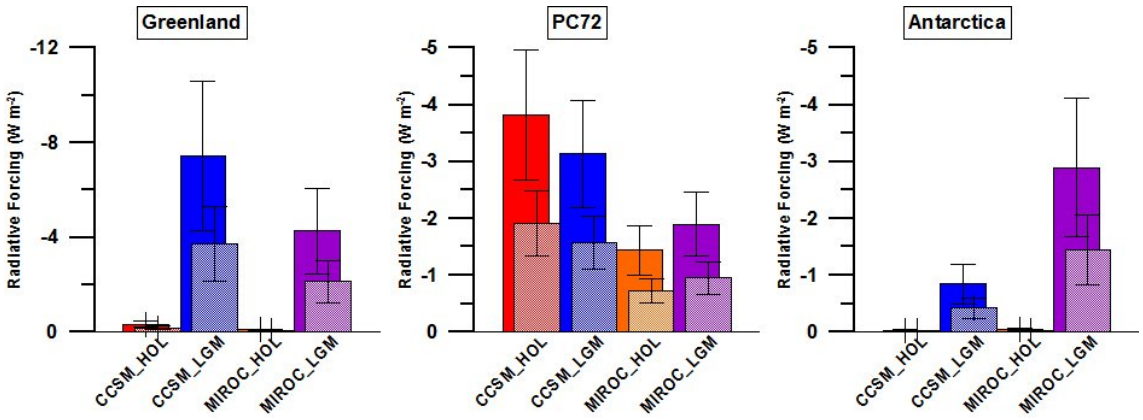

Fig. 3: Regional radiative forcing due to reconstructed atmospheric dust aerosol concentrations in Greenland and Antarctica. PC72 gives a low albedo comparison at low latitudes. The lower lightly colored bars represent the “MIN” scenario, whereas the higher fully colored bars show values calculated in the “MAX” scenario.

References:

1. Miller, R.L. & Tegen, I. Climate Response to Soil Dust Aerosols. *Journal of Climate* **11**, 3247-3267 (1998).

2. Martin, J.H., Gordon, R.M. & Fitzwater, S.E. The Case for Iron. *Limnology and Oceanography* **36**, 1793-1802 (1991).

3. Tegen, I. Modeling the mineral dust aerosol cycle in the climate system. *Quaternary Science Reviews* **22**, 1821-1834 (2003).

4. Mahowald, N.M. *et al.* Change in atmospheric mineral aerosols in response to climate: Last glacial period, preindustrial, modern, and doubled carbon dioxide climates. *Journal of Geophysical Research* **111**, (2006).

5. Takemura, T. *et al.* A simulation of the global distribution and radiative forcing of soil dust aerosols at the Last Glacial Maximum. *Atmospheric Chemistry and Physics* **9**, 3061-3073 (2009).

6. Mahowald, N.M. *et al.* Climate response and radiative forcing from mineral aerosols during the last glacial maximum, pre-industrial, current and doubled-carbon dioxide climates. *Geophysical Research Letters* **33**, 2-5 (2006).

7. Claquin, T. *et al.* Radiative forcing of climate by ice-age atmospheric dust. *Climate Dynamics* **20**, 193–202 (2003).

8. Lambert, F. *et al.* Dust-climate couplings over the past 800,000 years from the EPICA Dome C ice core. *Nature* **452**, 616-9 (2008).

9. Ruth, U., Wagenbach, D., Steffensen, J.P. & Bigler, M. Continuous record of microparticle concentration and size distribution in the central Greenland NGRIP ice core during the last glacial period. *Journal of Geophysical Research* **108**, 1-12 (2003).

10. Winckler, G., Anderson, R.F., Fleisher, M.Q., McGee, D. & Mahowald, N. Covariant glacial-interglacial dust fluxes in the equatorial Pacific and Antarctica. *Science* **320**, 93-6 (2008).

11. Sassen, K., Demott, P.J., Prospero, J.M. & Poellot, M.R. Saharan dust storms and indirect aerosol effects on clouds : CRYSTAL-FACE results.

Geophysical Research Letters **30**, 1-4 (2003).

12. Mahowald, N. *et al.* Dust sources and deposition during the last glacial maximum and current climate: A comparison of model results with paleodata from ice cores and marine sediments. *Journal of Geophysical Research* **104**, 15895–15 (1999).

13. Kohfeld, K.E. & Harrison, S.P. DIRTMAP: the geological record of dust. *Earth-Science Reviews* **54**, 81-114 (2001).

14. Maher, B. a. *et al.* Global connections between aeolian dust, climate and ocean biogeochemistry at the present day and at the last glacial maximum. *Earth-Science Reviews* **99**, 61-97 (2010).

15. Huang, S.P., Pollack, H.N. & Shen, P.-Y. A late Quaternary climate reconstruction based on borehole heat flux data, borehole temperature data, and the instrumental record. *Geophysical Research Letters* **35**, 1-5 (2008).

16. Tierney, J.E. *et al.* Northern Hemisphere Controls on Tropical Southeast African Climate During the Past 60,000 Years. *Science* **322**, 252-255 (2008).

17. Weijers, J.W.H., Schefuss, E., Schouten, S. & Sinninghe Damsté, J.S. Coupled thermal and hydrological evolution of tropical Africa over the last deglaciation. *Science* **315**, 1701-4 (2007).

18. Jouzel, J. *et al.* Orbital and millennial Antarctic climate variability over the past 800,000 years. *Science* **317**, 793-6 (2007).

19. Masson-Delmotte, V. *et al.* Past and future polar amplification of climate change: climate model intercomparisons and ice-core constraints. *Climate Dynamics* **26**, 513-529 (2005).

20. Alley, R.B. The Younger Dryas cold interval as viewed from central Greenland. *Quaternary Science Reviews* **19**, 213-226 (2000).

21. Graversen, R.G., Mauritsen, T., Tjernström, M., Källén, E. & Svensson, G. Vertical structure of recent Arctic warming. *Nature* **451**, 53-6 (2008).

22. Serreze, M.C. & Francis, J. a. The Arctic Amplification Debate. *Climatic*

Change **76**, 241-264 (2006).

23. Jansen, E. *et al.* Palaeoclimate. *Climate Change 2007: The Physical Science Basis. Contribution of Working Group I to the Fourth Assessment Report of the Intergovernmental Panel on Climate Change* (2007).

24. Albani, S., Mahowald, N.M., Delmonte, B., Maggi, V. & Winckler, G. Comparing modeled and observed changes in mineral dust transport and deposition to Antarctica between the Last Glacial Maximum and current climates. *Climate Dynamics* **Submitted**,

25. Gaiero, D. Iron and other transition metals in Patagonian riverborne and windborne materials: geochemical control and transport to the southern South Atlantic Ocean. *Geochimica et Cosmochimica Acta* **67**, 3603-3623 (2003).

26. Sun, J., Zhang, M. & Liu, T. Spatial and temporal characteristics of dust storms in China and its surrounding regions, 1960–1999: Relations to source area and climate. *Journal of Geophysical Research* **106**, 10325-10333 (2001).

27. Mahowald, N., Albani, S., Engelstaedter, S., Winckler, G. & Goman, M. Model insight into glacial–interglacial paleodust records. *Quaternary Science Reviews* **30**, 832-854 (2011).

28. Mlawer, E.J., Taubman, S.J., Brown, P.D., Iacono, M.J. & Clough, S. a. Radiative transfer for inhomogeneous atmospheres: RRTM, a validated correlated-k model for the longwave. *Journal of Geophysical Research* **102**, 16663-16682 (1997).

29. Mahowald, N.M. *et al.* Observed 20th century desert dust variability: impact on climate and biogeochemistry. *Atmospheric Chemistry and Physics* **10**, 10875-10893 (2010).

30. Dai, A. Drought under global warming: a review. *Wiley Interdisciplinary Reviews: Climate Change* **2**, 45-65 (2011).

31. Mahowald, N.M. Anthropocene changes in desert area: Sensitivity to climate model predictions. *Geophysical Research Letters* **34**, L18817 (2007).

Supplementary Information

Atmospheric dust concentration reconstruction

Flux to surface concentration calculation:

The flux of a stable (non-volatile) aerosol is the sum of it's dry and wet deposition:

$F = F_{wet} + F_{dry}$

Therefore

$F_{dry} = F - F_{wet} = F \bullet (1 - F_{wet} / F) = F \bullet d$

with

$d = 1 - F_{wet} / F = F_{dry} / F$ the dry deposition fraction of the total flux

The dry deposition flux is obtained by multiplying the surface concentration with the dry deposition velocity:

$F_{dry} = v_{dry} \bullet C_{air}$

Therefore, the surface concentration can be obtained with the three parameters F, d, v_{dry}:

$C_{air} = F_{dry} / v_{dry} = F \bullet d / v_{dry}$

Global reconstruction:

The DIRTMAP 3 database collects average dust mass accumulation rates

(MAR) from many sites around the world for both Holocene and LGM conditions[1]. Only the sites that are not flagged for contamination were considered. To be consistent with model data, only the PM10 fraction was used. Some MAR values that were published after the DIRTMAP 3 database were added to reach a total of 322 and 303 sites for Holocene and LGM conditions, respectively (Table T1).

The logarithmic values of the MAR at each location were then interpolated to a global grid using a kriging algorithm[2] (fig. S1). As the data values in the DIRTMAP dataset have uncertainties and we are generally interested in the total amount of dust flux in an area, we used block kriging instead of point kriging to allow a certain leeway in the interpolation. Dust is preferably distributed along meridional lines and not in a latitudinal direction. Therefore, the semi-variogram fit was optimized for the east-west direction, the north-south direction being fitted within the east-west constrains. The resulting global dust flux grid was then multiplied with the dry deposition fraction from each model, and divided by the modeled dry deposition velocity. To reflect the changes in particle size distribution at varying distance from the sources, MAR values below 0.1, between 0.1 and 10, and above 10 μg m^{-2} s^{-1} were divided by each

model's dry deposition velocity of particles with diameters around 1.5, 3, and 6 μm, respectively.

Reconstructed concentrations are generally higher than their model counterpart. Especially, the reconstructions feature a much more pronounced zonal distribution than the models (Fig. 1). Sensitivity tests with different variograms show that this is not an artifact from the interpolation, as the bands are not distributed in random directions.

Uncertainty estimation:

The absolute logarithmic and relative linear standard deviation of the dust flux resulting from the kriging interpolation is displayed for both Holocene and LGM conditions in Figure S1. Note that since we used block kriging this uncertainty represents the standard deviation of the average value of the rectangular blocks centered on the grid nodes, not of the nodes themselves. Also, the nugget effect in the semi-variogram was not set to zero to account for the uncertainty in the MAR data. For the Holocene, standard deviations are generally below 30% in areas around data-points. In areas with sparse data coverage the uncertainty goes up to 70% (northern Russia, Canada, southern Indian Ocean) with a peak

uncertainty of 100% in the South Pacific. Standard deviations during the LGM are generally below 50% on continental landmasses due to better data coverage thanks to loess deposits. However, ocean data are more sparse and uncertainties reach 100% in the mid-Pacific, the Indian Ocean and the South Atlantic. The South Pacific features a large region with no LGM data points and uncertainties reach peak values of 200% there.

There is an additional error that comes from the inherent problem when mapping a sphere on a rectangular grid. The interpolation was performed on a degree scale, but these do not represent a constant physical distance. Thus, the semi-variogram used in the kriging process is misrepresenting the distance between high-latitude data-points. As the overwhelming majority of data-points is in the low and mid-latitudes, the global effect is small. The polar dust fields may be somewhat distorted by this effect, but as they are not overly complicated to begin with, the potential for misrepresenting patterns is small.

The transformation of dust flux to surface concentrations requires a multiplication with the dry deposition factor and a division with the dry deposition velocity. These two variables are taken from the models, and their uncertainty

within each model difficult to assess. We have opted to do the calculations with both model's parameters and show both results. As more global dust simulations get performed, an ensemble mean with uncertainty can be calculated for both variables.

Distributions:

In figure S2 we show the distributions of the logarithm of the reconstructed surface concentrations in the six zonal bands and globally. In general, dust concentration counts can be well fitted with a log-normal (Gaussian) distribution. The mean of the distribution follows the pattern shown in table 1a with high dust loads in the low- and mid-latitudes, and low dust loads in polar areas. Zonal bands with a high degree of atmospheric latitudinal mixing will display a low standard deviation. Most zonal bands show this feature in both reconstructions with standard deviations between 0.5 and 0.7. LGM distributions are generally narrower than their Holocene counterpart, which is a consequence of the broader latitudinal mixing during cold periods. Some zonal bands point to a dual peak with a larger standard deviation. This dual behavior of the distributions shows a greater zonal disparity in zonal bands having regions with very different

dust loads (e.g. continental and ice sheet, desert and ocean, …).

Detailed polar reconstruction:

The detailed analysis uses remote sites in Greenland, Antarctica and the Pacific Ocean. These sites are far removed from potential local dust sources and their dust flux variations should represent the average background atmospheric dust load. The list of sites and references is given in table T2. Holocene and LGM average dust flux values for all sites were taken from ice core and marine sediment measurements. Holocene and LGM averages were taken from the period 8 kyr BP – 2 kyr BP and 26 kyr BP – 19 kyr BP, respectively. For NGRIP the Holocene period was chosen from 11.6 kyr BP to 10.4 kyr BP, as there are no dust data available prior to 10 kyr BP. A comparison with GRIP calcium data shows that Holocene dust deposition in central Greenland was comparable in the early and mid-Holocene.

As mentioned before, the surface concentrations are calculated by multiplying the dust flux with the dry deposition fraction and dividing by the dry deposition velocity. The dry deposition flux is defined as the gravitational settling of particles plus an additional flux coming from other processes like impaction,

interception, diffusion, etc. The dry deposition fraction was measured for present conditions in Greenland for Al and Ca at 0.3[3], and in Antarctica for continental (non sea salt) SO_4 at 0.8[4]. For LGM conditions, values of 0.7 and 0.9 were respectively assumed for Greenland and Antarctica, in accordance with both model's trend towards more dry deposition at high latitudes during the LGM[5–7]. In the equatorial Pacific site (PC72), each model's value was taken for both Holocene and LGM conditions (CCSM: 0.31 and 0.14 for Holocene and LGM, respectively[5], MIROC: 0.68 and 0.7 for Holocene and LGM, respectively[7]).

Based on ice core data, a particle diameter of 1.3 and 1.7 μm was assumed at NGRIP during the Holocene and LGM, respectively[8], while at GRIP these two values amounted to 1.6 and 1.9 μm[9]. In both Antarctic sites, a diameter of 2.08 and 1.91 μm was assumed for Holocene and LGM conditions, respectively[10]. In the equatorial Pacific site, an average background mode of 2 μm was assumed for both Holocene and LGM conditions. Each model's deposition velocity to particle size relationship was fitted with a quadratic fit (r^2 always >0.99) to deduce the deposition velocity for each site's specific particle size.

The vertical dust concentration profile over each site was obtained by scaling

the profiles from the CCSM and MIROC models to the reconstructed surface concentration for both Holocene and LGM conditions.

Uncertainty estimation:

Dust flux and the sediment data at PC72 have an uncertainty <30%[8,11,12].

We decided not to use the dry deposition ratios from the models as the model values do not match the measurements[3,4]. Also, models have traditionally performed rather poorly in polar latitudes. The Greenland value comes with a 50% uncertainty and one can assume a similar value for Antarctica and our LGM estimates, although the Antarctic uncertainty is probably lower. The calculated dry deposition flux therefore has an uncertainty of ~60%.

The model's uncertainty in dry deposition velocities is difficult to assess. Again we opted to show the results from both models independently until a sufficient number of dust models are published to perform ensemble means. The CCSM velocities are quite close to the Stokes velocity due to gravitational settling alone. The MIROC velocities are significantly higher and ascribe a greater importance to secondary effects. These two values should provide a minimum and maximum estimate of the dry deposition velocity and bracket the uncertainty due to secondary effects.

The uncertainty is unfortunately quite high, but could be significantly reduced by precise measurements of the dry deposition flux and velocities in Greenland, Antarctica, and over the ocean..

Seasonality:

Southern South America was identified as the major LGM source for dust in East Antarctica[13], with other sources possibly contributing during warm times[14]. Dust enthrallment in Southern South America appears to happen all year round, with a maximum in spring and summer[15–17]. Dust in Greenland and the equatorial Pacific originates in East Asia[6,18]. Dust emission in East Asia is strongly seasonal with peak activity centered in spring and to a lesser degree in summer[19–21]. In Greenland, seasonal changes were observed in dust deposition[22] with concentration in ice cores peaking during spring[23]. We can therefore assume that the atmospheric dust concentrations during polar summer were higher than during the winter, and that most of the deposition occurred during the polar summer. The exact summer fraction, however, may be difficult to quantify. We performed two calculations to bracket the two extreme cases. In the minimum case (MIN), we assumed lower surface

concentrations, as if dust was deposited evenly throughout the year. In the maximum case (MAX) we doubled the MIN surface concentrations as if all the dust was only deposited during polar summer. The polar radiative forcing (RF) calculations were conducted in average summer atmospheric conditions, whereas yearly averaged atmospheric conditions were used at the equatorial site.

Radiative Fluxes

Global calculations:

The direct RF (shortwave + longwave) has been estimated by comparing the zonal medians of the reconstructions (table 1a) with the modeled dust surface concentration to RF relationship (Fig. S2 to S5). RF and surface dust concentrations evolve relatively linearly (differences within a band occur due to varying surface albedo, topography, etc.), and in most cases a linear fit describes the relationship satisfactorily. Each reconstruction has been compared with it's respective model's data. We give an estimate of the uncertainty involved by declaring the range of the two values obtained by the two model's surface concentration to RF relationship. In some polar bands the

reconstructed surface concentrations were outside the range of the model values. In those cases we give no value (N/A) to the RF. However, to calculate the global RF average, the unknown polar RF was considered negligible compared to mid- and low-latitude RF, and set to zero.

A similar exercise with indirect RF showed no linear relationship between it and surface dust concentrations. We therefore make no refrain from estimating indirect RF at this point.

Detailed polar calculations:

In order to examine the role of dust in polar amplification during the LGM period, the shortwave direct RF due to atmospheric dust aerosols was calculated at the five locations in table T2 in clear sky conditions. The vertical profile of the dust-induced RF was calculated by feeding the profile of dust aerosol optical depth to a one-dimensional radiative transfer model[24]. The dust profile was converted to aerosol optical depth using a MIE scattering algorithm[25]. Mineral dust particles optical properties were set as described in the OPAC database[26]. The calculations are robust against changes in CO_2, O_3, relative humidity, and temperature in the atmosphere. The results were also not significantly altered

by substituting the National Center for Environmental Prediction's atmospheric data (NCEP 2) for any model's Holocene atmosphere. In figure 3 we show the average of the two Greenland and the two Antarctic sites. The error bars represent the uncertainty of the RF assuming a 60% error in the dust dry deposition flux at each site (As RF scales very linearly with surface concentrations in the 1-D model, we can transfer the dust uncertainty directly to the RF). A measure of uncertainty from the deposition velocity is indicated by the difference between the CCSM and MIROC models. In the case of the Pacific site, the error bars represent the 30% uncertainty in the total dust flux. The combined error from the model's dry deposition fraction and deposition velocity is illustrated by the difference in the respective results.

Longwave RF is always positive and usually a fraction of the shortwave forcing. However, unlike shortwave radiation, longwave radiation is heavily influenced by clouds at varying altitudes (ref). An adequate modeling of longwave RF would therefore require a dedicated polar atmospheric model and is beyond the scope of this study. Based on global dust models, the longwave warming may amount to 20-30% of the shortwave cooling at the surface[27].

Tables

Location	Longitude	Latitude	HOL MAR(g/m2/a)	LGM MAR(g/m2/a)	PM10 fraction	Citation
Bahia Blanca	-62.27	-38.72	26	N/A	N/A	Gaiero et al., 2004
Carpathian Basin	19.48	45.67	156	2700	0.23	Stevens et al., 2011
Comodoro Rivadavia	-67.48	-45.86	19	N/A	N/A	Gaiero et al., 2005
Corsica	9.08	45.15	12.25	N/A	N/A	Goudie et al., 2001
Hungary	21.57	47.53	205.63	N/A	0.23	Sumegi et al., 2007
Hungary	19.81	47.51	95.43	N/A	0.23	Sumegi et al., 2007
Hungary	21.37	48.15	244.60	N/A	0.23	Sumegi et al., 2007
Hungary	21.56	47.79	156.11	N/A	0.23	Sumegi et al., 2007
Hungary	21.36	48.8	91.87	N/A	0.23	Sumegi et al., 2007
Niger	6	15	200.00	600	N/A	Goudie et al., 2001
NGRIP	-42.32	75.1	0.008	0.17	N/A	Ruth et al., 2003
Talos Dome	159.18	-72.82	0.0013	0.0085	N/A	Delmonte et al., 2010
Pampas	-62	-33	28	N/A	N/A	Maher et al., 2010
Pampas	-62	-39	26	N/A	N/A	Maher et al., 2010
Puerto Madrin	-65.05	-42.77	55	N/A	N/A	Gaiero et al., 2003

Table T1: List of sites and MAR values added to the DIRTMAP 3 database[1,8,28–31].

SiteID	**Longitude °E**	**Latitude °N**	**Holocene Dust Flux mg m^{-2} yr^{-1}**	**LGM Dust Flux mg m^{-2} yr^{-1}**	**Reference**
NGRIP	-42.32	75.1	8	163	Ruth et al., 2003, Rasmussen (pers.com.)
GRIP	-37.63	72.58	9	326	Steffensen, 1997, Rasmussen (pers.com.)
TTN013-PC72	-139.4	0.1	168	332	Winckler et al., 2006
Dome C	123.21	-75.06	0.37	9.6	Lambert et al., 2008
Vostok	106.83	-78.46	0.58	12.2	Petit et al., 1999

Table T2: List and location of sites used in this study's detailed RF calculations[8,12,32,33].

Figures

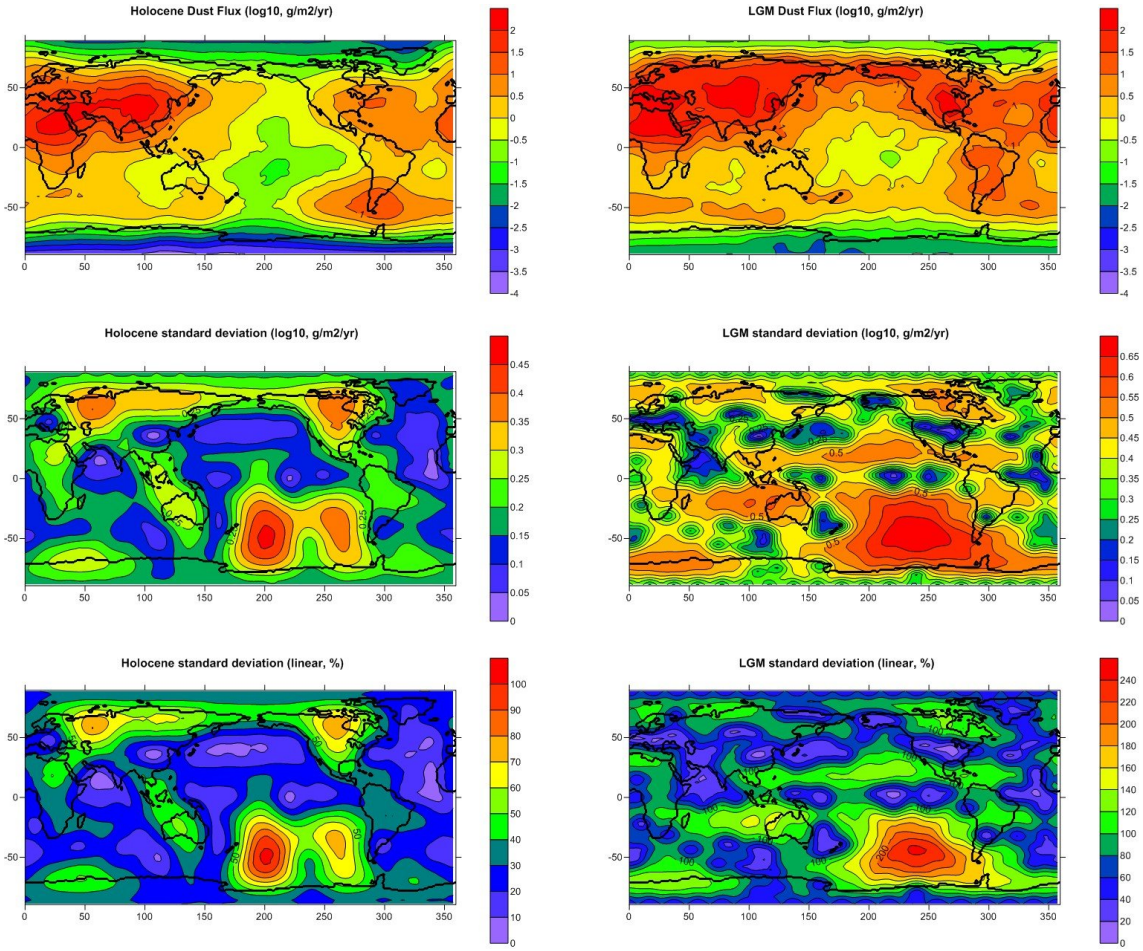

Fig. S1: Error of the kriging interpolation for Holocene and LGM conditions. The color bar marks the relative standard deviation.

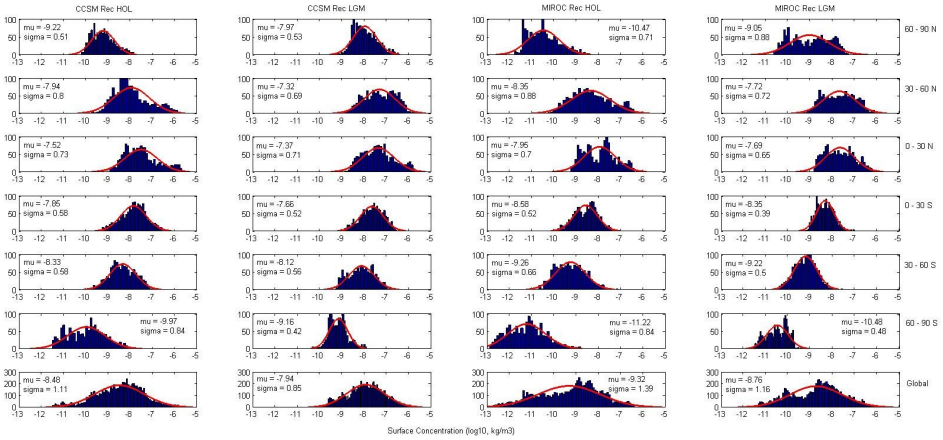

Fig S2: Zonal and global distributions of the logarithm of the reconstructed surface dust concentrations.

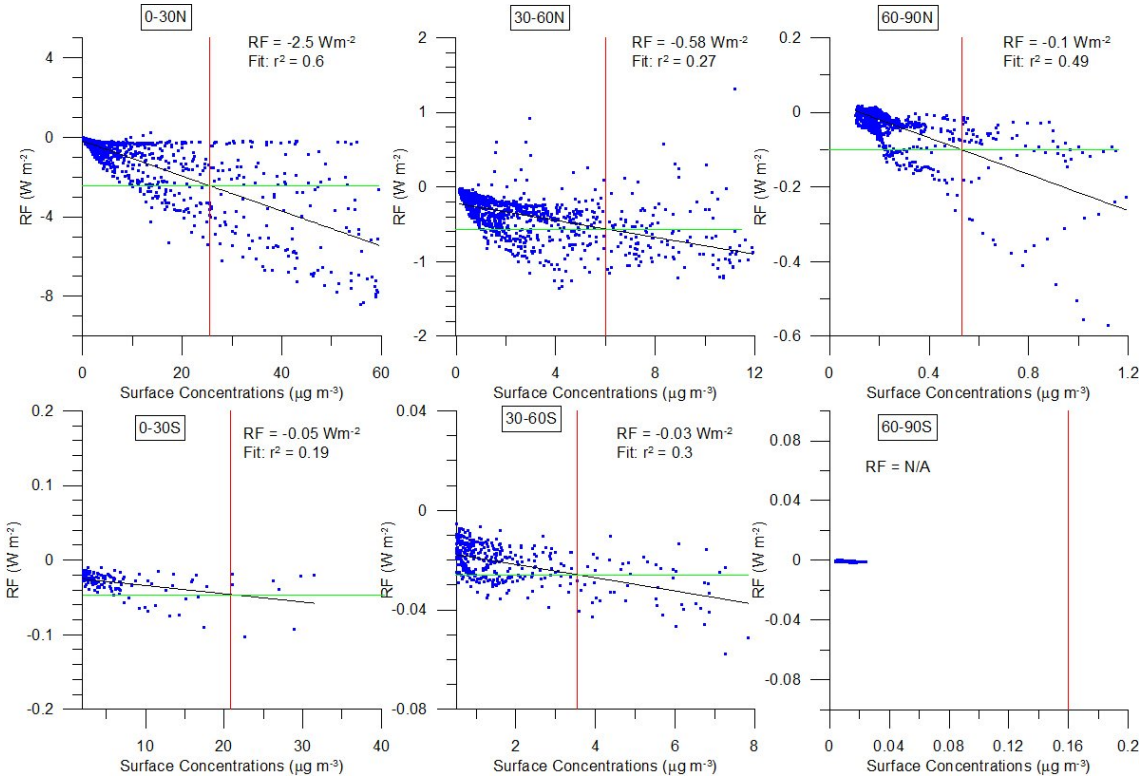

Fig. S3: Relationship of CCSM surface concentrations with direct RF (SW+LW) during Holocene conditions[34]. The zonal average of the CCSM-reconstruction is displayed as a red line. The green line marks the estimated corresponding RF.

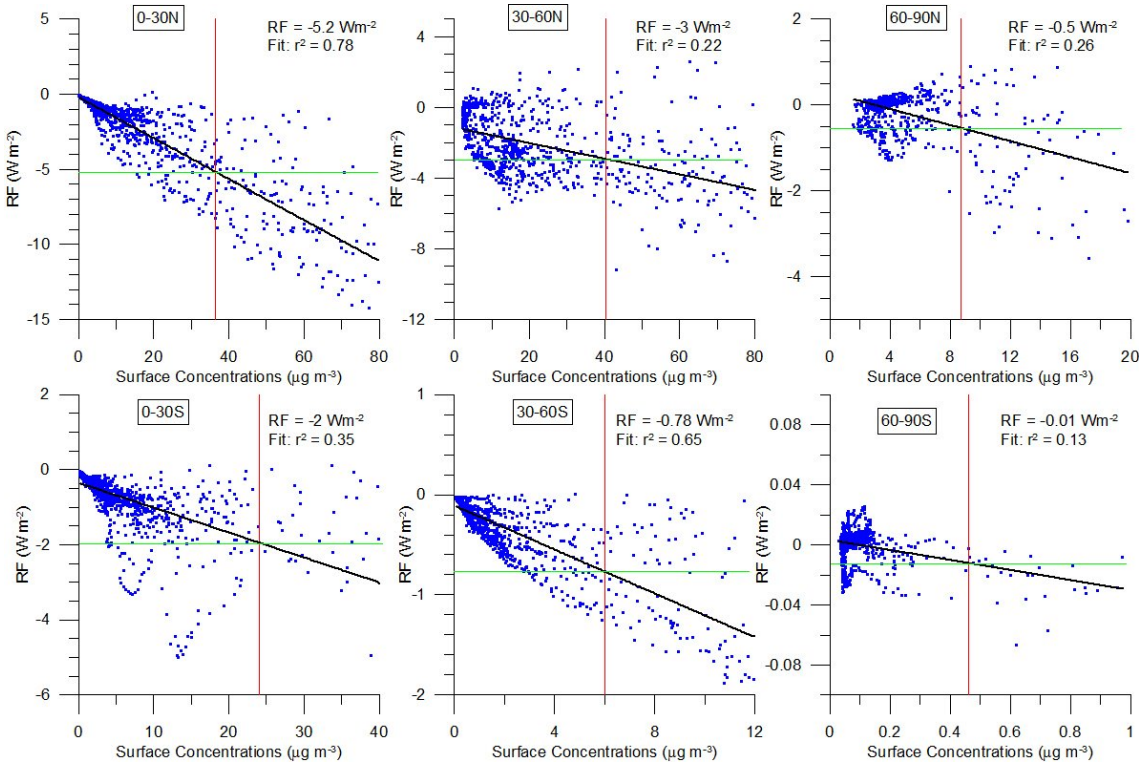

Fig. S4: Relationship of CCSM surface concentrations with direct RF (SW+LW) during LGM conditions[34]. The zonal average of the CCSM-reconstruction is displayed as a red line. The green line marks the estimated corresponding RF.

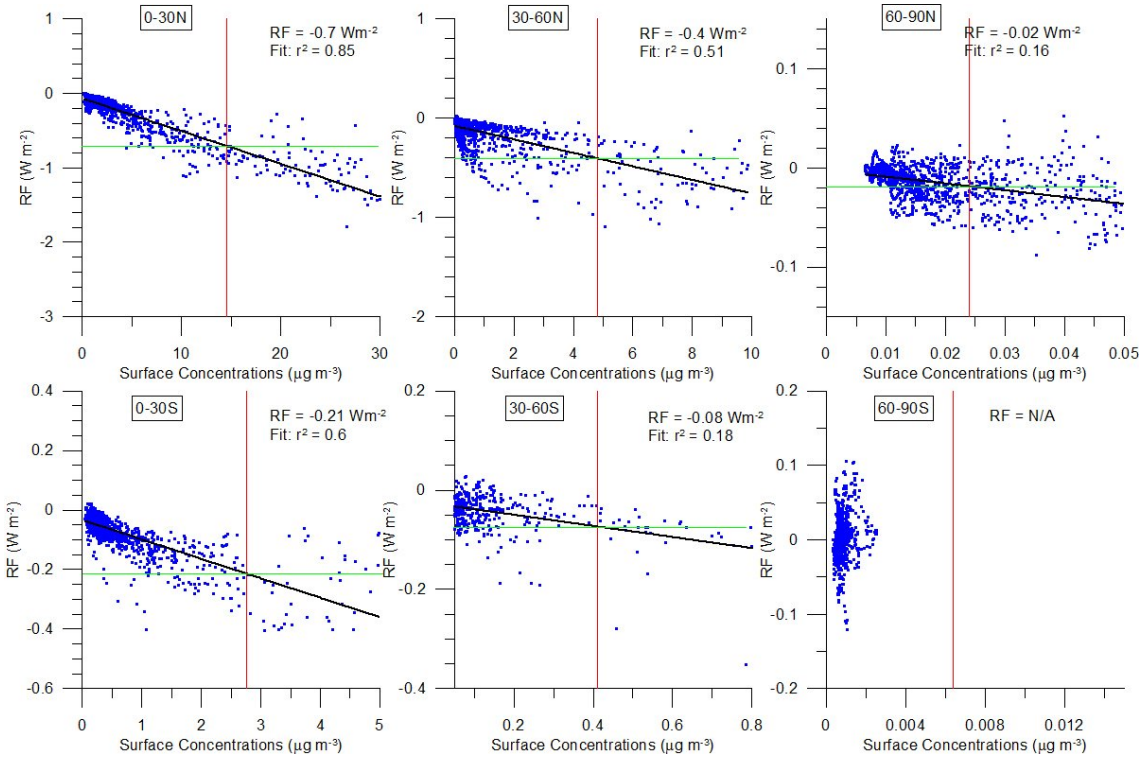

Fig. S5: Relationship of MIROC surface concentrations with direct RF (SW+LW) during Holocene conditions[7]. The zonal average of the MIROC-reconstruction is displayed as a red line. The green line marks the estimated corresponding RF.

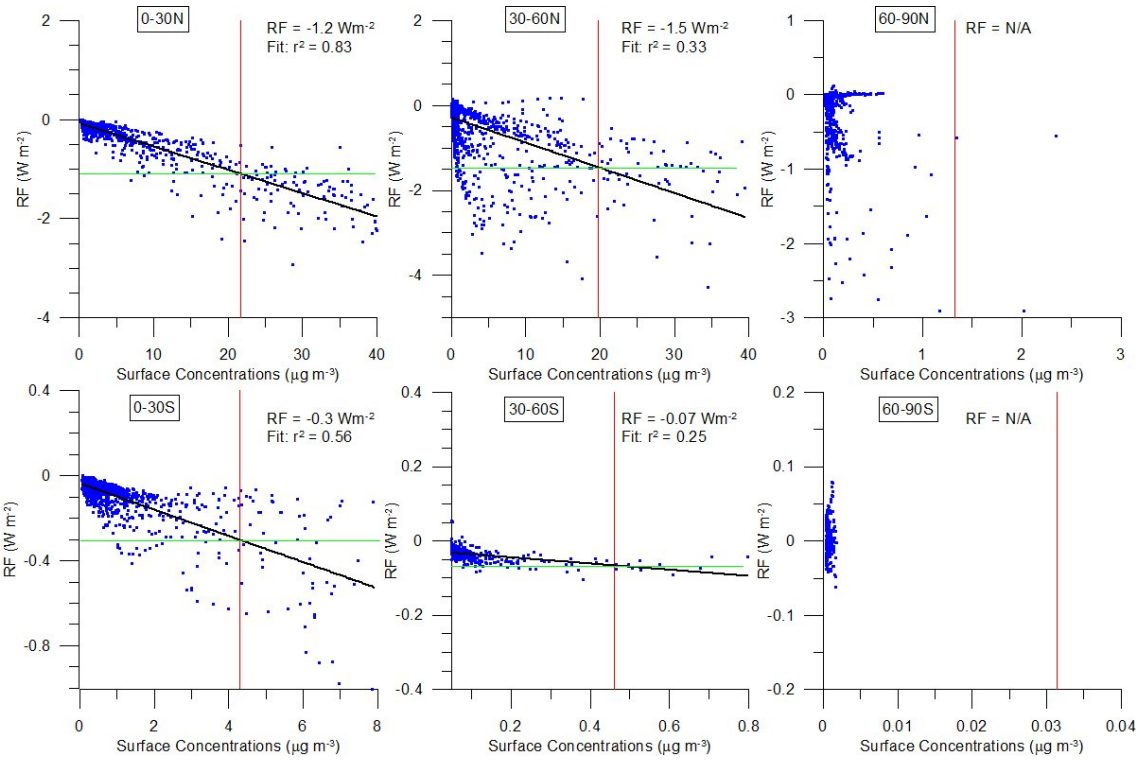

Fig. S6: Relationship of MIROC surface concentrations with direct RF (SW+LW) during LGM conditions[7]. The zonal average of the MIROC-reconstruction is displayed as a red line. The green line marks the estimated corresponding RF.

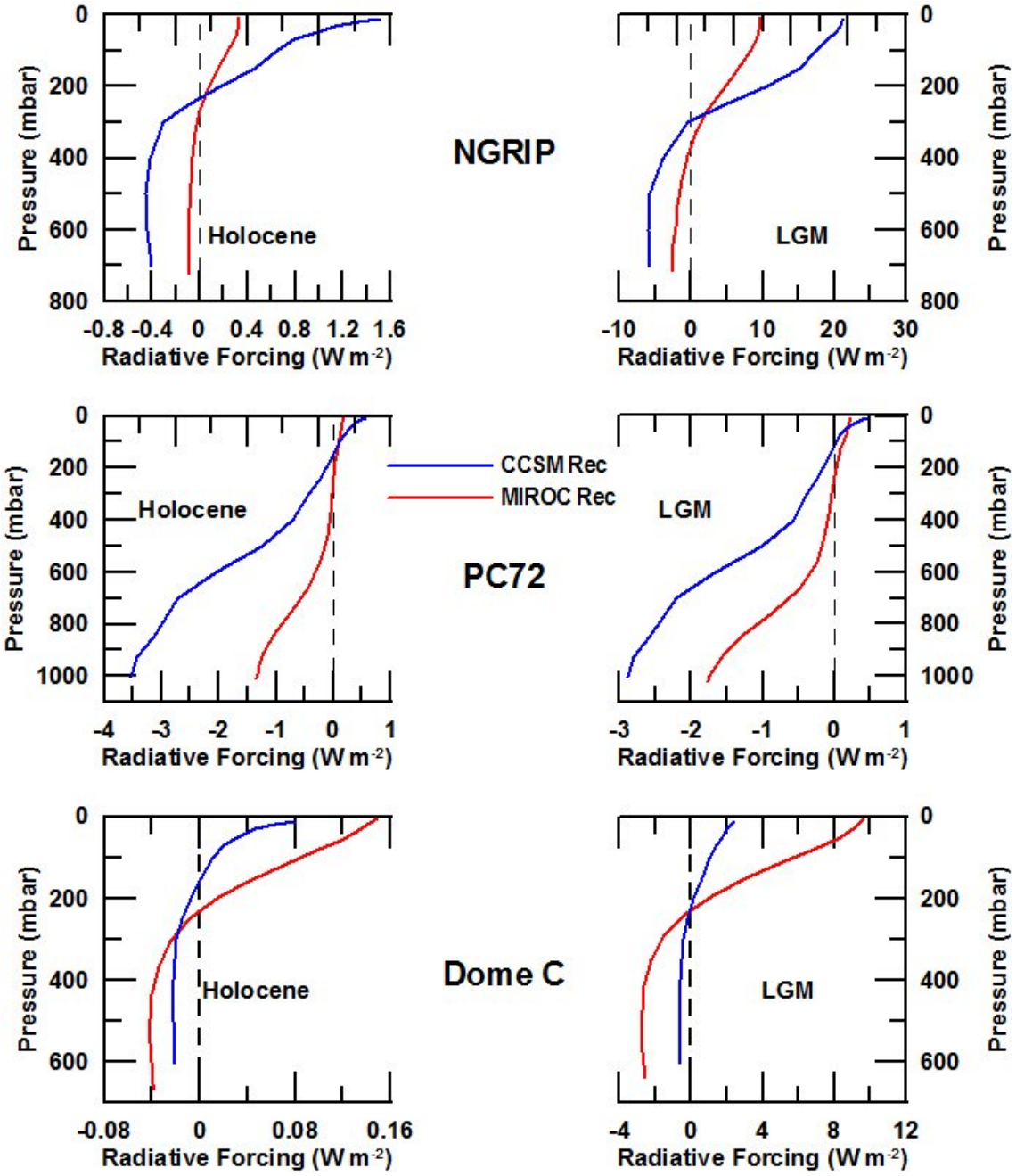

Fig. S7: Radiative forcing due to dust at three representative sites under Holocene and LGM conditions. The calculations were performed using dust concentrations corresponding to the MAX scenario described in the text.

References

1. Maher, B. a. *et al.* Global connections between aeolian dust, climate and ocean biogeochemistry at the present day and at the last glacial maximum. *Earth-Science Reviews* **99**, 61-97 (2010).

2. Cressie, N. *Statistics for Spatial Data*. (John Wiley and Sons, Inc., New York: 1991).

3. Davidson, C. *et al.* Chemical constituents in the air and snow at Dye 3, Greenland–I. Seasonal variations. *Atmospheric Environment. Part A. General Topics* **27**, 2709–2722 (1993).

4. Wolff, E.W. *et al.* Southern Ocean sea-ice extent, productivity and iron flux over the past eight glacial cycles. *Nature* **440**, 491-6 (2006).

5. Mahowald, N.M. *et al.* Change in atmospheric mineral aerosols in response to climate: Last glacial period, preindustrial, modern, and doubled carbon dioxide climates. *Journal of Geophysical Research* **111**, (2006).

6. Mahowald, N., Albani, S., Engelstaedter, S., Winckler, G. & Goman, M. Model insight into glacial–interglacial paleodust records. *Quaternary Science Reviews* **30**, 832-854 (2011).

7. Takemura, T. *et al.* A simulation of the global distribution and radiative forcing of soil dust aerosols at the Last Glacial Maximum. *Atmospheric Chemistry and Physics* **9**, 3061-3073 (2009).

8. Ruth, U., Wagenbach, D., Steffensen, J.P. & Bigler, M. Continuous record of microparticle concentration and size distribution in the central Greenland NGRIP ice core during the last glacial period. *Journal of Geophysical Research* **108**, 1-12 (2003).

9. Steffensen, J.P. The size distribution of microparticles from selected segments of the Greenland Ice Core Project ice core representing different climatic periods. *Journal of Geophysical Research* **102**, 26755–26 (1997).

10. Delmonte, B., Petit, J.R. & Maggi, V. Glacial to Holocene implications of the new 27000-year dust record from the EPICA Dome C (East Antarctica) ice

core. *Climate Dynamics* **18**, 647-660 (2002).

11. Jouzel, J. *et al.* Orbital and millennial Antarctic climate variability over the past 800,000 years. *Science* **317**, 793-6 (2007).

12. Winckler, G., Anderson, R.F., Fleisher, M.Q., McGee, D. & Mahowald, N. Covariant glacial-interglacial dust fluxes in the equatorial Pacific and Antarctica. *Science* **320**, 93-6 (2008).

13. Delmonte, B. *et al.* Comparing the Epica and Vostok dust records during the last 220,000 years: stratigraphical correlation and provenance in glacial periods. *Earth-Science Reviews* **66**, 63-87 (2004).

14. Revel-Rolland, M. *et al.* Eastern Australia: A possible source of dust in East Antarctica interglacial ice. *Earth and Planetary Science Letters* **249**, 1-13 (2006).

15. Albani, S., Mahowald, N.M., Delmonte, B., Maggi, V. & Winckler, G. Comparing modeled and observed changes in mineral dust transport and deposition to Antarctica between the Last Glacial Maximum and current climates. *Climate Dynamics* **Submitted**,

16. Gaiero, D. Iron and other transition metals in Patagonian riverborne and windborne materials: geochemical control and transport to the southern South Atlantic Ocean. *Geochimica et Cosmochimica Acta* **67**, 3603-3623 (2003).

17. Gassó, S. & Stein, A.F. Does dust from Patagonia reach the sub-Antarctic Atlantic Ocean? *Geophysical Research Letters* **34**, 1-5 (2007).

18. Biscaye, P.E. *et al.* Asian provenance of glacial dust (stage 2) in the Greenland Ice Sheet Project 2 Ice Core, Summit, Greenland. *Journal of Geophysical Research* **102**, 26765-26781 (1997).

19. Xuan, J. & Sokolik, I.N. Characterization of sources and emission rates of mineral dust in Northern China. *Atmospheric Environment* **36**, 4863-4876 (2002).

20. Sun, J., Zhang, M. & Liu, T. Spatial and temporal characteristics of dust storms in China and its surrounding regions, 1960–1999: Relations to source area and climate. *Journal of Geophysical Research* **106**, 10325-

10333 (2001).

21. Natsagdorj, L., Jugder, D. & Chung, Y.S. Analysis of dust storms observed in Mongolia during 1937-1999. *Atmospheric Environment* **37**, 1401-1411 (2003).

22. Hammer, C. *et al.* Dating of Greenland ice cores by flow models, isotopes, volcanic debris, and continental dust. *Journal of Glaciology* **20**, 3–26 (1978).

23. Rasmussen, S.O. *et al.* A new Greenland ice core chronology for the last glacial termination. *Journal of Geophysical Research* **111**, 1-16 (2006).

24. Mlawer, E.J., Taubman, S.J., Brown, P.D., Iacono, M.J. & Clough, S. a. Radiative transfer for inhomogeneous atmospheres: RRTM, a validated correlated-k model for the longwave. *Journal of Geophysical Research* **102**, 16663-16682 (1997).

25. Wiscombe, W.J. Improved Mie scattering algorithms. *Applied optics* **19**, 1505–1509 (1980).

26. Hess, M., Koepke, P. & Schult, I. Optical Properties of Aerosols and Clouds: The Software Package OPAC. *Bulletin of the American Meteorological Society* **79**, 831-844 (1998).

27. Yue, X., Wang, H., Liao, H. & Fan, K. Simulation of dust aerosol radiative feedback using the GMOD: 2. Dust-climate interactions. *J. Geophys. Res* **115**, 1-16 (2010).

28. Stevens, T., Marković, S.B., Zech, M., Hambach, U. & Sümegi, P. Dust deposition and climate in the Carpathian Basin over an independently dated last glacial–interglacial cycle. *Quaternary Science Reviews* **30**, 662-681 (2011).

29. Goudie, a. S. & Middleton, N.J. Saharan dust storms: nature and consequences. *Earth-Science Reviews* **56**, 179-204 (2001).

30. Sumegi, P. *et al.* Results of Radiocarbon Analysis of Upper Weichselian Loess Sequences from Hungary. *Radiocarbon* **49**, 1023-1030 (2007).

31. Delmonte, B. *et al.* Aeolian dust in the Talos Dome ice core (East Antarctica,

Pacific/Ross Sea sector): Victoria Land versus remote sources over the last two climate cycles. *Journal of Quaternary Science* **25**, 1327-1337 (2010).

32. Petit, J.R. *et al.* Climate and atmospheric history of the past 420,000 years from the Vostok ice core, Antarctica. *Nature* **399**, 429-436 (1999).

33. Lambert, F. *et al.* Dust-climate couplings over the past 800,000 years from the EPICA Dome C ice core. *Nature* **452**, 616-9 (2008).

34. Mahowald, N.M. *et al.* Climate response and radiative forcing from mineral aerosols during the last glacial maximum, pre-industrial, current and doubled-carbon dioxide climates. *Geophysical Research Letters* **33**, 2-5 (2006).